Millimetre-Wave Astronomy

Study Notes

John Garrett

Contents

1. Introduction

The millimetre (mm) and submillimetre (submm) wavelength spectrums are vital to understanding the cool universe. Whereas main-sequence stellar spectrums often peak in the visible band, black body radiation from the cool universe ($T \lesssim 100$ K) peaks in the mm- and submm-bands along with many of the important molecular spectral lines. In cold molecular clouds, these spectral lines include transitions such as the $J+1 \rightarrow J$ rotational lines of CO, HCN, HCO+, and other heavy molecules. Imaging these clouds is of great interest because from these measurements we are able to probe the chemical and physical properties present within **star forming regions**. This is crucial for understanding galaxy formation, evolution and dynamics; stellar evolution; and cosmology.

Receivers based on **superconductor-insulator-superconductor (SIS)** junctions are the current gold standard for measuring mm-and submm-wave spectral lines (from roughly 100 GHz to 1 THz). Direct-detection methods also exist, but only heterodyne receivers such as SIS mixers provide the necessary spectral resolution, $\lambda/\Delta\lambda \approx 10^6$, for measuring spectral line profiles and their Doppler shifts [1]. Heterodyne detectors also have the added advantage that they can be combined in large arrays through interferometry. Such observatories include the Atacama Large Millimetre Array (ALMA), Harvard's Submillimeter Array (SMA), IRAM's Northern Extended Millimetre Array (NOEMA), and CalTech's Combined Array for Research in Millimetre-Wave Astronomy (CARMA).

SIS mixers are a form of **heterodyne mixing**. These receivers operate by mixing the signal-of-interest (ω_s) with a strong, single-frequency signal called the local-oscillator (ω_{LO}). This shifts the spectral content of the signal-of-interest down to a frequency[1], ω_{IF}, that is favourable for digital processing. For example, a signal centered on 230 GHz may be down-converted to ∼5 GHz by mixing with a 225 GHz local-oscillator. No digital spectrometers are able to sample at 460 GHz (the Nyquist sampling rate for 230 GHz), but they certainly can at ∼5 GHz. The heterodyne receiver shown in Figure 1.1 is a dual sideband (DSB) receiver meaning that signals at $\omega_{LO} - \omega_{IF}$ and $\omega_{LO} + \omega_{IF}$ are down-converted to the same frequency.

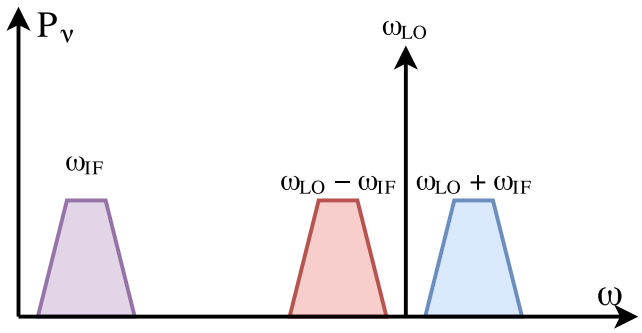

Figure 1.1.: The heterodyne mixing spectrum of a dual sideband receiver. Here, the red and blue RF spectrums are down-converted to the same purple IF spectrum.

The performance of heterodyne receivers is typically characterised by three **figures-of-merit**: (1) the **loss in power** resulting from the frequency translation, (b) the **noise added** per unit bandwidth, and (b) the **instantaneous bandwidth**. Note that the noise added per unit bandwidth is typically described by the noise temperature, $T_N = P_\nu/k$, of the mixer. This has a lower, quantum limit that is imposed by the Heisenberg uncertainty principle, $T_N > T_Q = h\nu/k$. In an ideal receiver, the conversion loss and noise temperature are kept as low as possible to maximise the receiver's sensitivity. For the same reason,

[1]This frequency is called the intermediate frequency (IF) signal. This is a legacy term that goes back to Edwin Armstrong and the invention of superheterodyne receivers. The idea is that this is an intermediate signal between the mixing component and the following filtering, amplification, integration, etc.

the instantaneous bandwidth is kept as large as possible, which also helps to increase the survey depth when measuring spectral sources.

Despite SIS technology being relatively mature, there is always a need for more sensitivity. This leads to shorter integration times and faster imaging speeds. The signal-to-noise ratio (S/N) of a heterodyne receiver is described by the Dicke radiometer equation,

$$\frac{S}{N} = \frac{T_A}{T_{sys}}\sqrt{\Delta\nu\Delta t}. \tag{1.1}$$

where T_A is the source's antenna temperature, T_{sys} is the receiver's noise temperature, $\Delta\nu$ is the instantaneous bandwidth, and Δt is the integration time. The sensitivity of a receiver can therefore be improved through any of these factors. The noise temperature of state-of-the-art SIS receivers however is already approaching the quantum limit, and any additional improvements are becoming increasingly difficult.

...not finished...

2. Radio Astronomy

2.1. Introduction

Radio astronomy is the study of celestial objects in the radio-frequency (RF) spectrum, which is traditionally defined as 3 kHz to 300 GHz. Practically however, ground-based radio astronomy extends from ∼10 MHz, below which the ionosphere blocks all radiation, to ∼1.5 THz where H_2O and N_2 molecules begin to absorb RF radiation [2].

Radio and optical astronomy differ in many regards, but the fundamental difference is the frequency of the light being observed. Through the **Planck–Einstein relation**, $E = h\nu$, this means that there is also a difference in the photon energy. For example, a photon at 400 MHz has less than $1/1{,}000{,}000^{\text{th}}$ of the energy of a red, visible-light photon. In optical astronomy, photons are typically used to generate charge through the photoelectric effect. In radio astronomy, the photons no longer have enough energy to overcome the binding energy in semiconductors. Instead, the radiation needs to be coupled to an electric circuit where the signal can be amplified, down-converted, filtered, and sampled. We therefore think of the radiation as EM waves instead of photons, as in the case of optical astronomy.

Despite radio astronomy merely being a different subset of the electromagnetic spectrum from optical astronomy, there are many differences in the physical properties that are observed and the technology that is used to make the observations. Many physical phenomena are only able to be understood in the radio spectrum, therefore radio astronomy is necessary for a comprehensive study of astrophysics.

2.2. Signals in Radio Astronomy

In traditional radio communication, information signals are modulated with carrier signals to shift the spectral content of the information to such a frequency that it can be transmitted wirelessly. The result is a strong, coherent signal where the signal at time $t + \Delta t$ is strongly correlated to the signal at time t. An example is amplitude modulated (AM) radio where the audio signal (20 Hz to 5 kHz) is modulated with a carrier (single tone between 500–1,700 kHz) so that it can be transmitted over the air. The result is a sine-wave carrier with a time-varying envelope that contains audio information (Figure 2.1).

The radio emission from celestial objects however is **incoherent**, meaning that the phase at time $t + \Delta t$ is unrelated to the phase at t. **Celestial signals therefore appear as random noise** (Figure 2.1) and they are indistinguishable from the thermal noise of a resistor[1]. From the source's measured power spectrum (P_ν, in SI units W Hz^{-1}), we can then define T_{source} as the noise temperature of the source:

$$T_{source} \equiv \frac{P_{\nu,source}}{k} \tag{2.1}$$

T_{source} will be indistinguishable from all other sources of thermal noise including thermal emission from the ground, atmosphere and telescope optics, and the thermal noise of the receiver circuit itself. The overall signal that is measured (T_{meas}) will then be the combination of all of these noise sources (in SI units K):

$$\begin{aligned} T_{meas} &= T_{source} + T_{gnd} + T_{atm} + T_{receiver} + T_{cmb} + ... = \frac{P_{\nu,meas}}{k} \\ &= T_{source} + T_{sys} \end{aligned} \tag{2.2}$$

[1] Also called Johnson, Nyquist, or Johnson-Nyquist noise.

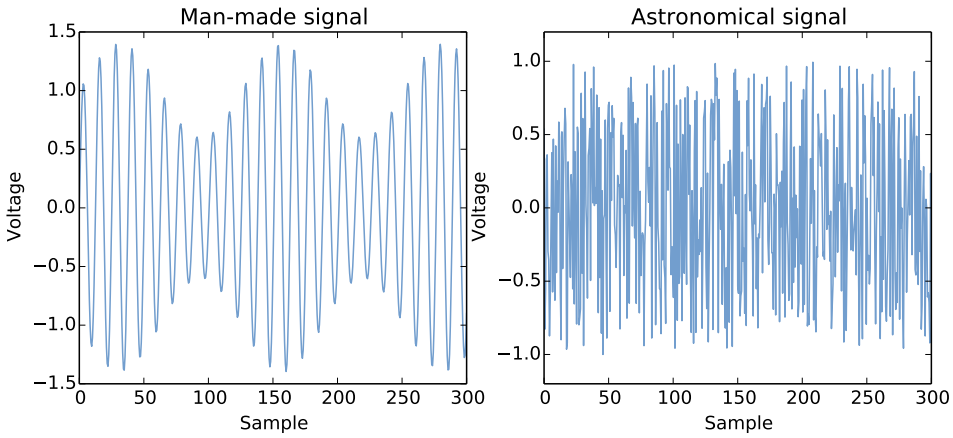

Figure 2.1.: The difference between man-made and astronomical signals.

In Equation 2.2, T_{sys} represents the noise temperature of the entire system. Since $T_{source} + T_{sys}$ is the combination of many different noise sources, through the **central limit theorem** we know that this noise will have a **Gaussian distribution**. Note that T_{source} is typically several orders of magnitude weaker than the overall value for T_{meas}.

2.2.1. Measuring Thermal Noise

Thermal noise will have an average voltage of 0 (i.e., $\langle v \rangle = 0$), but a non-zero RMS value (v_{rms}) and therefore non-zero power. To measure the average noise power, a **radiometer** is used. The simplest radiometer consists of:

1. an **antenna** to couple freespace EM radiation to the electric circuit,
2. a **bandpass filter** to select a subset of the frequency spectrum ($\nu_{RF} - \Delta\nu/2$ to $\nu_{RF} + \Delta\nu/2$),
   - $\Delta\nu$ is the instantaneous bandwidth (the range of frequencies that will be measured simultaneously). In a heterodyne receiver, this is called the intermediate-frequency (IF) bandwidth.
   - After the bandpass filter, the signal will no longer look random. It will appear as a signal modulated at ν_{RF} with an envelope that varies on timescales of $\sim \Delta\nu^{-1}$.
3. a **square-law detector**[2] to generate a signal that is proportional to the input noise power,
   - $v_{out} \propto v_{in}^2 \;\; \therefore \;\; v_{out} \propto P_{in}, \;\; \langle v_{out} \rangle \neq 0$
   - the frequency of the oscillating component $\sim 2\nu_{RF}$
4. an **integrator** to smooth out any fluctuations in v_{out}, and finally
   - Integrate for $\Delta t \gg (\Delta\nu)^{-1}$ (a low pass filter).
5. a **voltometer** to measure v_{out}.

After integrating for time Δt at the Nyquist rate[3], there will be $N = \Delta t / T_{sample} = 2\Delta\nu\Delta t$ independent samples of T_{sys}, each with $\sigma_T \approx \sqrt{2}T_{sys}$ RMS error. This error will reduce as more samples are gathered and averaged together:

$$\sigma_T = \frac{\sqrt{2}T_{sys}}{\sqrt{N}} \tag{2.3}$$

By plugging in the value for N,

[2]The simplest square-law detector is a diode.

[3]Nyquist sampling theorem: To fully sample a signal, samples must be taken at double the signal's frequency bandwidth. Note that it is double the instantaneous bandwidth ($\Delta\nu$), not just the highest frequency contained within the signal.

$$\sigma_T \approx \frac{T_{sys}}{\sqrt{\Delta\nu \cdot \Delta t}} \tag{2.4}$$

the **Dicke radiometer equation** is found. T_{source} should be $\gtrsim 5 \cdot \sigma_T$ for a well-defined detection (i.e., the signal-to-noise ratio should be > 5).

Note that Equation 2.4 implies that an arbitrarily large S/N can be achieved. In reality, systematic errors limit the ability to integrate over long periods of time. For example, if **gain instability** is included, equation 2.4 becomes:

$$\sigma_T \approx T_{sys} \left[\frac{1}{\Delta\nu \cdot \Delta t} + \left(\frac{\Delta G}{G} \right)^2 \right]^{1/2} \tag{2.5}$$

which puts a lower bound on σ_T. **Atmospheric fluctuations** will also cause a similar effect.

Both of these can be corrected through **Dicke switching**. This involves switching between the source and an empty patch of sky a few beam widths away (so that the beam is going through roughly the same atmosphere). Then when integrating, the power is multiplied by +1 when the beam is on the source, and by -1 when it is on the empty sky. The average power should then remain constant. Since the beam is only on the source for half the time however, σ_T will be twice as large.

2.2.2. Measuring the System Noise Temperature

The noise temperature of receiver systems is typically characterised by measuring the system's response to hot and cold loads, at T_H and T_C, respectively. The system's output power from these loads (P_H and P_C, respectively) will be proportional to the input temperature (with a zero offset due to noise) provided that the load temperatures are within the Rayleigh-Jeans approximation ($h\nu/kT$). The noise temperature of the system is then:

$$T_{sys} = \frac{T_H - T_C\, Y}{Y - 1} \tag{2.6}$$

where $Y = P_H/P_C$ and is often called the Y-factor.

2.3. Black Body Radiation

Planck's law gives the spectral density of electromagnetic radiation emitted by an ideal black body in thermodynamic equilibrium:

$$B_\nu(T) = \frac{2h\nu^3}{c^2} \frac{1}{e^{\frac{h\nu}{kT}} - 1} \tag{2.7}$$

$$B_\lambda(T) = \frac{2hc^2}{\lambda^5} \frac{1}{e^{\frac{hc}{k\lambda T}} - 1} \tag{2.8}$$

Aside

Note that I_ν and B_ν are used interchangeably for spectral radiance (also known as specific intensity, spectral intensity, spectral brightness, or just generally brightness), which is the energy per unit time per unit area per unit frequency per unit solid angle. In SI units, this is J $s^{-1}m^{-2}Hz^{-1}sr^{-1}$. A steradian (sr) is the SI unit for solid angle. One steradian is defined as:

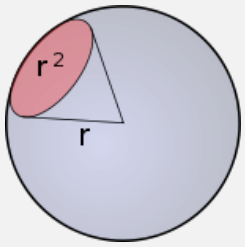

An entire sphere is 4π steradians or roughly 12.5 sr.

The peak of the blackbody spectrum is given by **Wien's displacement law**,

$$\frac{\nu_{\max}}{\text{GHz}} = 58.789 \left(\frac{T}{K}\right). \tag{2.9}$$

For low frequencies (such as those in radio astronomy), $h\nu/kT \ll 1$. Then using

$$\frac{1}{e^{\frac{h\nu}{kT}} - 1} \approx \frac{kT}{h\nu}, \tag{2.10}$$

Equation 2.7 reduces to

$$B_\nu(T) = \frac{2\nu^2}{c^2} kT \tag{2.11}$$

which is **Rayleigh-Jeans law**. The difference between Planck's law and the Rayleigh-Jeans approximation becomes apparent as ν approaches the peak of the black body radiation curve (Figure 2.2).

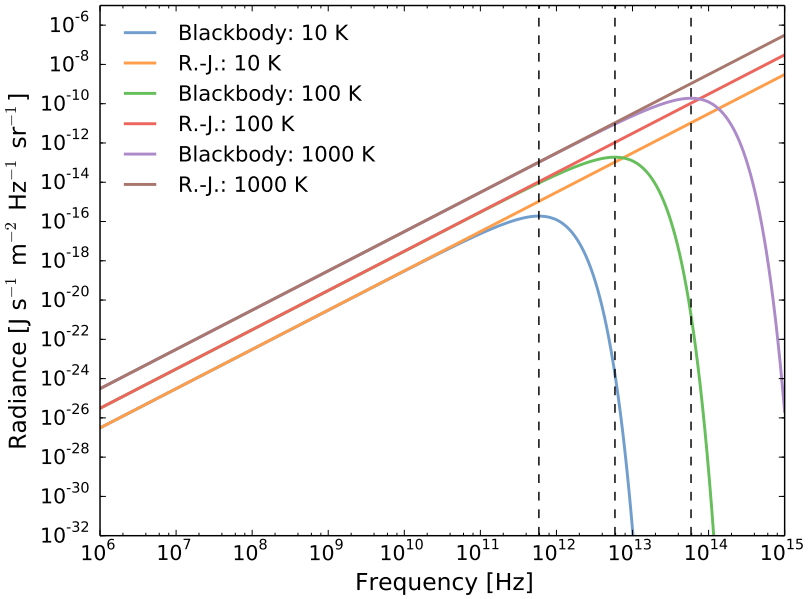

Figure 2.2.: Black body spectral radiance for 10, 100, and 1000 K. The dashed lines mark the peaks of the black body curves.

Aside

In radio astronomy, we often pretend that sources are thermal (i.e., $I \propto \nu^2$) even when they're not. By rearranging Equation 2.11, we can define brightness temperature (T_b):

$$T_b(\nu) \equiv \frac{c^2}{2k\nu^2}\frac{1}{\nu^2}I_\nu = \frac{\lambda^2}{2k}I_\nu \tag{2.12}$$

If the signal is thermal and within the Rayleigh-Jeans limit, $T_b(\nu)$ will be constant. This will not be true for other emission (e.g., free-free, synchrotron).

Integrating the spectral radiance over all frequencies and solid angles gives the power per unit area (i.e., the radiant emittance), also known as **Stefan-Boltzman's law**:

$$j^* = P/A = \sigma T^4, \quad \sigma = \frac{2\pi^4 k^4}{15c^2h^3} \tag{2.13}$$

$$\therefore \; P \propto T^4 \tag{2.14}$$

In the case of a star (or any spherical object with radius R), j^* can be integrated over the surface to determine the total bolometric power (energy per unit time):

$$L_{bol} = 4\pi R^2 \sigma T^4 \tag{2.15}$$

2.4. Measuring Black Body Radiation

To figure out how much energy will be measured with a telescope, we can integrate the spectral radiance over solid angle, frequency and area:

$$P_{measured} = \iiint I_\nu \; d\Omega \; dA \; d\nu \tag{2.16}$$

It is important to note that the **spectral radiance (I_ν) is conserved (is constant) along any line of sight in empty space.** Therefore, I_ν is independent of distance, and it is the same at the source as it is at the detector. Spectral radiance can be thought of as energy flowing out of the source, or energy flowing into the detector [3] as shown in Figure 2.3.

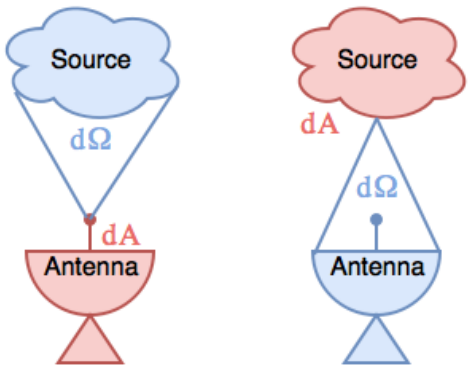

Figure 2.3.: Two ways to think about spectral radiance.

If a source is discrete (meaning that it occupies a defined solid angle), the **flux density** (S_ν, in units W m^{-2} Hz^{-1}) at the telescope can be found:

$$S_\nu = \int_{source} I_\nu \, d\Omega \tag{2.17}$$

Aside

The SI unit for flux density [W m^{-2} Hz^{-1}] is far too large for any astronomical source. Instead, Janskys are used where 1 Jy $= 10^{-26}$ W m^{-2} Hz^{-1}. Even then milli-Janskys are often needed!

The **flux**[4] can also be found (F, in SI units W m^{-2}):

$$F = \int I_\nu \, d\Omega \, d\nu = \int S_\nu \, d\nu \tag{2.18}$$

Note that flux and flux density *do* depend on distance through the inverse square law:

$$S_\nu \propto 1/d^2, \quad F \propto 1/d^2 \tag{2.19}$$

The total power measured by the telescope will then be $P = F \, A_{eff}$ where A_{eff} is the effective aperture area of the telescope. This ignores efficiency losses. Including polarisation and efficiency losses (η), Equation **??** becomes:

$$P = \frac{1}{2}\eta F A \tag{2.20}$$

To find the total power per unit frequency (units W Hz^{-1}) that a source is radiating, we can extend the flux density over the entire sphere to determine the **spectral luminosity** (L_ν, in units W Hz^{-1}):

$$L_\nu = \int S_\nu \, dA = 4\pi d^2 S_\nu \tag{2.21}$$

The **bolometric luminosity** (L_{bol}, in units W, sum of all radiation emitted from the source) is then defined as:

$$L_{bol} \equiv \int_0^\infty L_\nu \, d\nu \tag{2.22}$$

2.5. Radio Antennas

Most radio antennas use parabolic dishes to increase the directivity of the beam. However, even an ideal dish will be diffraction limited:

$$\Omega_A \approx \frac{\pi}{4}\theta^2 \approx \frac{\pi}{4}\left[\frac{4\lambda}{\pi D}\right]^2 = \frac{4}{\pi}\frac{\lambda^2}{D^2} \approx \frac{\lambda^2}{D^2} \tag{2.23}$$

[4] Radiative flux. This is different from other definitions of flux such as magnetic flux $\Phi_B = \iint \mathbf{B} \cdot d\mathbf{S}$.

Aside

The general equation to determine the beam solid angle of an antenna is:

$$\Omega_A = \int_{\text{sphere}} |F(\theta,\phi)|^2 \, d\Omega = \int_{\text{sphere}} P(\theta,\phi) \, d\Omega \tag{2.24}$$

where $F(\theta,\phi) = E/E_{\max}$ is the normalised field pattern and P is the normalised power pattern (a.k.a., the beam pattern).
For an aperture antenna (e.g., waveguide horn or parabolic dish), the narrowest beam (minimum Ω_A/maximum directivity) is obtained when the E-field is uniform across the aperture. This gives:[a]

$$\Omega_A = \frac{\lambda^2}{A_p} = \frac{\lambda^2}{\pi(D/2)^2} = \frac{4}{\pi}\frac{\lambda^2}{D^2} \approx \frac{\lambda^2}{D^2} \tag{2.25}$$

The solid angle of a narrow cone (where the spherical cap's area is approximately the area of the base of the cone) is given by:

$$\Omega \approx \frac{\pi}{4}\theta^2 \tag{2.26}$$

The angular diameter θ of the uniform aperture antenna is then roughly $\theta \approx \frac{4\lambda}{\pi D}$ which is close to the well-known diffraction limit equation for circular apertures: $\theta \approx 1.22\frac{\lambda}{D}$.

[a] For proof see sec. 9.5 of "Antenna Theory and Design" by W. Stutzman and F. Thiele.

The measured flux density for an extended source[5] within the R.-J. limit will be:

$$S_\nu = \int I_\nu \, d\Omega = I_\nu \, \Omega_A \tag{2.27}$$

This can be integrated across the surface of the dish to find the **power spectral density (PSD):**

$$P_\nu = \frac{1}{2} I_\nu \Omega_A A_p \tag{2.28}$$

$$= \frac{1}{2}\frac{2\nu^2 kT}{c^2}\frac{4\lambda^2}{\pi D^2}\frac{\pi D^2}{4} \tag{2.29}$$

$$= kT \tag{2.30}$$

Aside

Johnson-Nyquist or thermal noise describes the noise in a resistor due to the random thermal motion of the electrons. It is typically written as:

$$v_n = \sqrt{4kTR\Delta f} \tag{2.31}$$

Or in terms of power spectral density as:

$$P_\nu = kT \tag{2.32}$$

The **power spectrum (P_ν) can therefore be described by a noisy resistor!** We can then set the power spectrum equal to

$$T_a \equiv \frac{P_\nu}{k} \tag{2.33}$$

where T_a is called the **antenna temperature**. Since T_a represents our signal, we can combine Equation 2.33 with Equation 2.4 to get the signal-to-noise ratio (S/N):

[5] Extended source: the source's beam solid angle Ω_s is larger than Ω_A.

$$\frac{S}{N} = \frac{T_a}{T_{sys}}\sqrt{\Delta v\ \Delta t} \tag{2.34}$$

In this ideal case, the antenna temperature will be equal to the brightness temperature (T_b). Real systems will have non-ideal beam patterns, losses, polarisation mismatch, and sources which can be smaller than the beam pattern. Therefore, $T_a \leq T_b$. For a source (Ω_S) that is smaller than the beam solid angle (Ω_A), the antenna temperature will be lower than the brightness temperature.

$$T_A \approx T_B \frac{\Omega_S}{\Omega_A} \tag{2.35}$$

The ratio Ω_S/Ω_A is known as the **beam filling factor.**

2.6. Heterodyne Receivers

Most radio astronomy telescopes use heterodyne receivers. This is because heterodyne receivers preserve phase information (important for interferometry) and provide extremely high spectral resolution ($\lambda/\Delta\lambda \approx 10^6$, limited by the backend). The block diagram for a millimetre-wave, heterodyne receiver is shown in Figure 2.4. Most radio receivers place filters and low-noise amplifiers (LNAs) as the first elements in the receiver chain, but LNAs don't exist yet in the millimetre-wave spectrum.

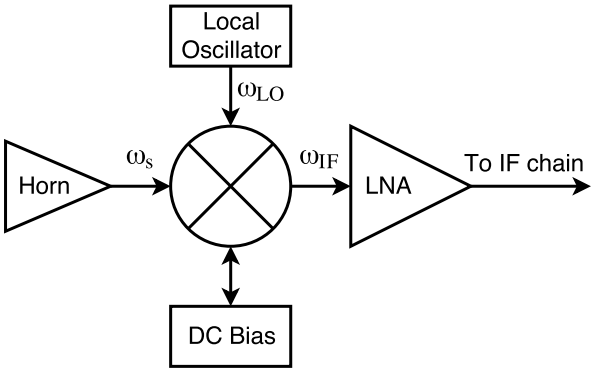

Figure 2.4.: Block diagram of a heterodyne receiver. Mixers are traditionally represented by $\otimes$ in circuit diagrams.

Due to the way noisy components cascade,

$$T_{sys} = T_1 + \frac{T_2}{G_1} + \frac{T_3}{G_1 G_2} + ... \tag{2.36}$$

$$T_{sys} \approx T_M + G_M^{-1}\ T_{IF} \tag{2.37}$$

the noise properties of the first in line components are the most important (the first components the signal encounters). Therefore, the noise temperature of the mixer (T_M) and the low-noise amplifier (T_{IF}) must be as low as possible, and the mixer's gain (G_M) should be kept close to 0 dB. Since the gain of the LNA is very high ($\sim$ 30 dB), T_{IF} is dominated by the noise from the LNA.

All heterodyne mixers are limited by Heisenberg's uncertainty principle,

$$T_Q = \frac{hf}{k} = \frac{\hbar\omega}{k} \sim 11 \text{ K at } 230 \text{ GHz} \tag{2.38}$$

since the phase is maintained through this process

Acknowledgements

In writing this chapter, I used several books and papers [2, 4] as well as lecture notes from NRAO [5, 3] and Mike Jones at the University of Oxford.

3. Quantum Mechanics

3.1. Introduction

The initial interest in quantum mechanics came from the investigation of blackbody radiation and the photoelectric effect. The basics of blackbody radiation were already covered in Section 2.3, but the history is summarised below:

- 1860: **"Perfect black bodies"** are introduced by Gustav Kirchhoff. These theoretical objects absorb all incident light (i.e., nothing is reflected and nothing is transmitted through).
- 1900: Based on resonant modes in classical mechanics, the **Rayleigh-Jeans law** predicts the radiated power spectrum of a perfect black body:

$$B(\lambda, T) = \frac{2c}{\lambda^4}\, kT \tag{3.1}$$

  This law however predicts that radiated energy will increase unbounded as the frequency increases (the **ultraviolet catastrophe**). This shows a major failure of classical mechanics.
- 1900: Max Planck discovers his empirical formula,

$$B(\lambda, T) = \frac{C}{\lambda^5} \cdot \frac{1}{e^{c/\lambda T} - 1} \tag{3.2}$$

  where c and C are constants used for fitting to experimental data. In the following years, Planck developed the idea of quantised emission[1].
- 1905: Albert Einstein discovers quanta of light, now known as photons, during his work on the photoelectric effect. Each photon has an energy given by the **Planck-Einstein relation**:

$$E = h\nu \tag{3.3}$$

3.2. Schrödinger Equation and Wave Functions

In quantum mechanics, everything that is possible to know about about a particle is contained within its **wave functions**, Ψ. The **time-dependent Schrödinger equation** can then be used to describe how the wave function evolves over time[2]:

$$i\hbar \frac{\partial}{\partial t}\Psi(x,t) = \hat{H}\Psi(x,t) \tag{3.4}$$

where $\hat{H}$ is the **Hamiltonian operator**:

$$\hat{H} = -\frac{\hbar^2}{2m}\Delta^2 + V(x,t) \tag{3.5}$$

[1] Planck was reluctant to accept that absorption was quantised as well, and disagreed with Einstein's conclusions from the photoelectric effect. It wasn't until around 1919 that Planck accepted that both emission and absorption of light were quantised.

[2] This section roughly follows [6].

Aside

What does the wave function mean? There are several interpretations. According to **Born's statistical interpretation**, the wave function represents the probability of finding the particle in a given position, e.g., between $x = a$ and b:

$$P_{ab} = \int_a^b |\Psi(x,t)|^2 \, dx = \int_a^b \Psi(x,t) \cdot \Psi^*(x,t) \, dx \tag{3.6}$$

According to the **Copenhagen intrepretation**[a], the particle has no position until a measurement is made and the wave function collapses. Currently, the most popular interpretation is the **many-world interpretation** where the wave function never collapses.

[a] Attributed to Bohr and Heisenberg.

Since $|\Psi|^2$ represents a probability density function, the wave function must be normalised:

$$\int_{-\infty}^{+\infty} |\Psi(x,t)|^2 \, dx = 1 \tag{3.7}$$

3.2.1. Operators

The expectation value $\langle x \rangle$ will change over time. How fast it changes will determine its velocity,

$$\langle v \rangle = \frac{d\langle x \rangle}{dt} \tag{3.8}$$

Momentum ($p = mv$):

$$\langle p \rangle = m\frac{d\langle x \rangle}{dt} = -i\hbar \int \left(\Psi^* \frac{\partial \Psi}{\partial x} \right) \, dx \tag{3.9}$$

Operators (Q) are used to determine certain quantitites:

$$\langle Q(x,p) \rangle = \int \Psi^* \, Q\left(x, \frac{\hbar}{i}\frac{\partial}{\partial x} \right) \, \Psi \, dx \tag{3.10}$$

3.2.2. The Uncertainty Principle

Consider two waveforms:

1. A sine wave, which has a very well defined wavelength, but no obvious 'position'.
2. A Gaussian curve, which has a very well defined position, but no obvious wavelength.

This is the basic idea behind the uncertainty principle. Wavelength is related to momentum through the **de Broglie** relation:

$$p = \frac{h}{\lambda} = \frac{2\pi\hbar}{\lambda} \tag{3.11}$$

Heisenberg uncertainty principle:

$$\sigma_x \sigma_p \geq \frac{\hbar}{2} \tag{3.12}$$

3.3. The Time-Independent Schrödinger Equation

How do you determine Ψ? Use the Schrödinger equation with some specified potential, $V(x,t)$. If we assume that $V(x,t)$ is independent of time, t, we can separate Ψ into position and time components:

$$\Psi(x,t) = \psi(x)\varphi(t) \tag{3.13}$$

4. Normal Metals

Before moving on to superconductors and superconducting detectors, it is important to first understand where the resistance comes from in normal metals. This will be done by investigating simplified models of metals: the Drude model and the Drude–Sommerfeld model (a.k.a., the free electron model).

4.1. The Drude Model

In 1900, Paul Drude proposed his model of electrical conduction in metals. This model was proposed in the same year that Max Planck offered his solution to the black-body radiation problem (kick starting quantum mechanics). As such, this model does not incorporate quantum mechanics and instead treats electrons in a classical sense as a kinetic gas. Despite this, the model was very successful in modelling many of the different properties of metals (although unsuccessful in modelling some).

As mentioned, the Drude model assumes that the electrons in a metal can be treated as a kinetic gas. This means that electrons are assumed to travel freely in straight lines until they collide with nuclei. In between collision, the electrons are assumed to not interact with the fields of other electrons (**the independent electron approximation**) nor the fields of the nuclei (**free electron approximation**). The collisions are assumed to be instantaneous, and the velocity after a collision being unrelated to the velocity prior to that collision. The average time between collisions is called the **relaxation time** or mean free path time (τ), and it is only through these collisions that electrons achieve thermal equilibrium. A simple diagram is shown in Figure 4.1.

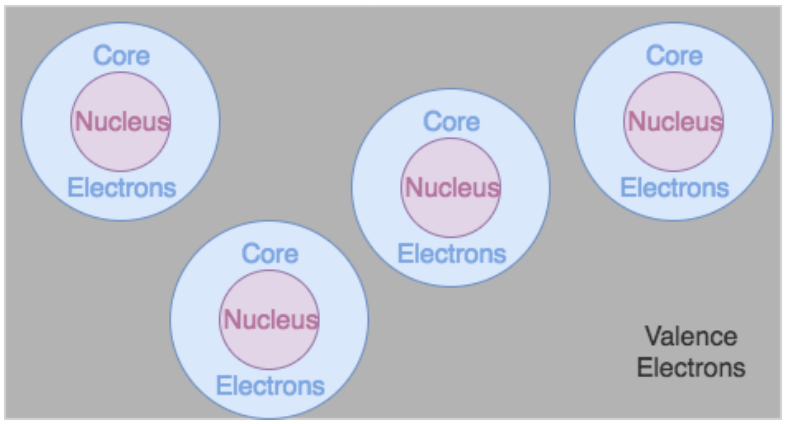

Figure 4.1.: The Drude model of a metal consists of an ion lattice (nuclei plus core electrons) with a free electron gas occupying the space in between.

4.1.1. DC Conductivity

Electrons will accelerate in an electric field ($\mathbf{E}$) as:

$$\mathbf{a} = -\frac{e}{m_e}\mathbf{E} \tag{4.1}$$

In a real metal however, the electrons won't be able to accelerate indefinitely because they will occasionally scatter off of the ion lattice. Recall that in the Drude model, an electron's velocity after a collision is completely unrelated to its velocity prior to the collision. These post-collision random velocities cancel

out, and all that's left is the acceleration due to the electric field in between collisions. The average velocity of the electrons then becomes:

$$\mathbf{v_{avg}} = -\frac{\tau e}{m_e}\mathbf{E} \tag{4.2}$$

This can be used to determine the current density ($\mathbf{j}$):

$$\mathbf{j} = -ne\mathbf{v_{avg}} = \frac{ne^2\tau}{m_e}\mathbf{E} \tag{4.3}$$

where $n = N/V$. Then using the definition of conductivity (σ),

$$\boxed{\mathbf{j} = \sigma\mathbf{E}} \tag{4.4}$$

the **DC conductivity** ($\sigma_0 = 1/\rho$) can be found:

$$\boxed{\sigma_0 = \frac{ne^2\tau}{m_e}} \tag{4.5}$$

4.1.2. Time-Varying Forces

If an external, spatially uniform force $\mathbf{f}(t)$ is applied (e.g., an electric or magnetic field), the momentum of the electrons will evolve as

$$\frac{d\mathbf{p}(t)}{dt} = -\frac{\mathbf{p}(t)}{\tau} + \mathbf{f}(t) \tag{4.6}$$

Note that this equation takes into account the odds of the electrons colliding with the lattice during the time step dt. Equation 4.5 can be found by substituting $\mathbf{f}(t) = -e\mathbf{E}$ and applying $\mathbf{p}(t) = -\frac{m_e}{ne}\mathbf{j}(t)$.

4.1.3. Hall Effect

If electrons flow in a wire in the positive x-direction and a magnetic field is applied in the positive z-direction, the Lorentz force

$$\mathbf{F} = q(\mathbf{E} + \mathbf{v} \times \mathbf{B}) \tag{4.7}$$

will cause the electrons to be deflected in the negative y-direction. As the electrons move in the negative y-direction, an electric field ($-E_y$) will be created to balance the motion of the electrons. Since the density of electrons is increasing on one side of the wire, the resistance will increase. The **magnetoresistance** is defined as:

$$\rho(H) = \frac{E_x}{j_x} \tag{4.8}$$

Hall determined that this quantity depends on the magnetic field. The quantity known as the Hall coefficient can also be defined as

$$R_H = \frac{E_y}{j_x H_z} \tag{4.9}$$

Aside

This effect can be used to build magnetometers[a] (a.k.a., Hall effect probes).

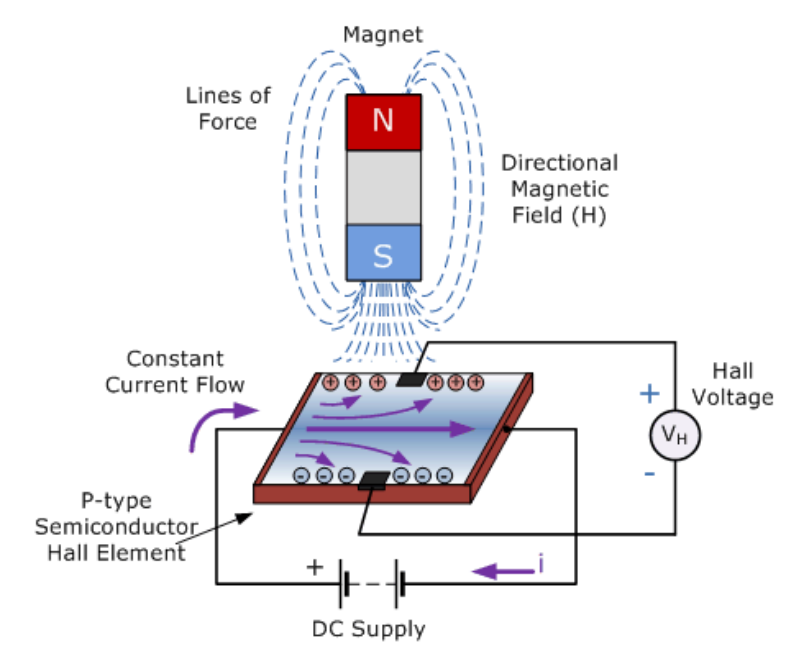

where the Hall voltage (V_H) is given by

$$V_H = R_H \left(\frac{I}{t} \, B \right) \tag{4.10}$$

and t is the thickness of the sensor.

[a]Figure from http://www.electronics-tutorials.ws/electromagnetism/hall-effect.html

The general form of Equation 4.6 in the presence of magnetic and electric fields can then be written as

$$\frac{d\mathbf{p}(t)}{dt} = -e \left(\mathbf{E} + \frac{\mathbf{p}(t) \times \mathbf{B}}{m_e} \right) - \frac{\mathbf{p}(t)}{\tau} \tag{4.11}$$

4.2. Drude–Sommerfeld Model

The Drude model was very successful for many years. For example, it successfully estimated the DC and AC conductivities of metals and the Hall effect. However, it provided drastically different values the specific heat capacity of metals than what was actually measured. This is because the energy distribution in the Drude model follows the Maxwell-Boltzmann distribution for kinetic gases, when in reality it should follow the Fermi-Dirac distribution. Sommerfeld corrected this in his model.

Similar to the Drude model, a metal in the Drude–Sommerfeld model consists of a positively-charged lattice (nuclei plus core electrons) and a gas of non-interacting, free electrons (a.k.a., the Fermi gas) filling the space in between. The electrons are able move around freely; however, since they are confined to the interior of a metal, the system can be seen as electrons trapped in a potential well. As such, they can only possess certain quantised energies states. For a cube with sides of length L, the wavefunctions are given by:

$$\Psi(n_x, n_y, n_z) = A \sin \frac{n_x \pi x}{L} \sin \frac{n_y \pi y}{L} \sin \frac{n_z \pi z}{L} \tag{4.12}$$

where n_x, n_y, n_z are positive integers and are all equal to one for the ground state (i.e., $n_x = n_y = n_z = 1$).

The kinetic energy of any state can be found through

$$E_K = \frac{\hbar^2 \pi^2}{2mL^2} \left(n_x^2 + n_y^2 + n_z^2\right) \tag{4.13}$$

At $T = 0$, the electrons will fill all of the lowest quantised energy states, with two electrons of opposite spin in each state. The highest energy of any state at $T = 0$ will be the **Fermi energy** [1] (E_F).

$$E_F = \frac{\hbar^2}{2m_e} (3\pi^2 n)^{\frac{2}{3}} \tag{4.14}$$

Note that an electron with the maximum kinetic energy will travel at the Fermi velocity ($\mathbf{v_F}$) with the Fermi wave vector ($\mathbf{k_F}$) and Fermi momentum ($\mathbf{p_F}$).

$$\mathbf{p_F} = m\mathbf{v_F} = \hbar \mathbf{k_F} \tag{4.15}$$

In momentum- or k-space, this will appear as a sphere of radius k_F.

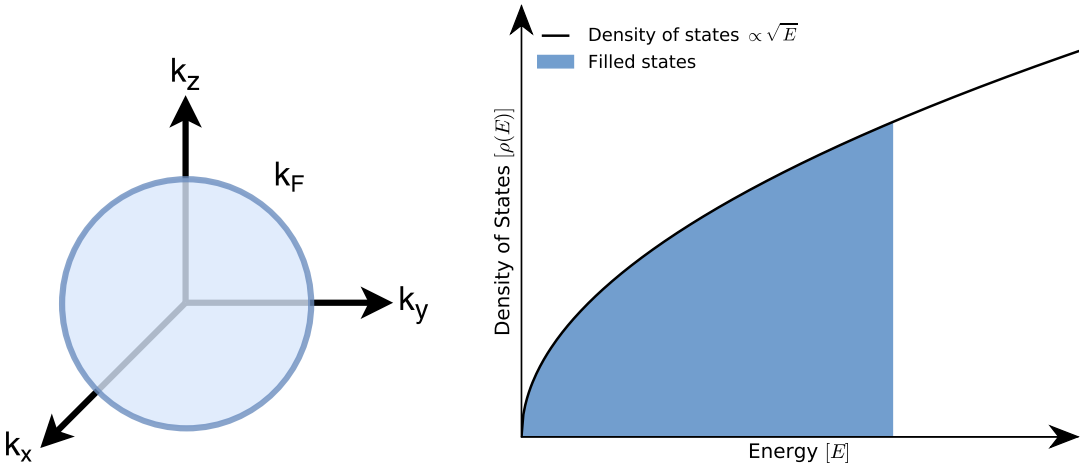

Figure 4.2.: Density of states for a normal metal at $T = 0$ K.

The momentum and velocity are related through:

$$E_F = \frac{1}{2} p_F v_F \tag{4.16}$$

When a voltage is applied, electrons will begin flowing through the lattice. If the lattice is perfect and completely still (as it would be at $T = 0$ K), the resistance will be zero. Note that at $T = 0$, since the Fermi sea's surface is completely flat, electrons aren't able to drop to a lower energy level and therefore can't scatter. Real metals however have imperfections and impurities which will cause scattering and a finite resistance even at $T = 0$ K. This resistivity is called the residual resistivity (ρ_i).

Aside

The mean distance between the scattering events is called the **electron mean free path length** (l_e). The resistivity is related to l_e through:

$$\rho_i = \frac{m v_F}{n e^2 l_e} \tag{4.17}$$

For $T > 0$, the Fermi surface will no longer be completely flat and electron scattering is possible (i.e., an electron is able to lose kinetic energy and drop to a lower unoccupied energy level). The probability that a certain state is filled is given by the **Fermi function**:

[1] Not to be confused with Fermi level.

$$f(E) = \frac{1}{e^{(E-E_F)/kT} + 1} \tag{4.18}$$

Figure 4.3 shows the Fermi function for a metal at room temperature. Note that at $T = 0$, Equation 4.18 reduces to a step function. Also note that it is only the electrons around E_F that scatter and contribute to electrical resistance since the electrons deeper in the Fermi sea are unable to drop to lower energy levels.

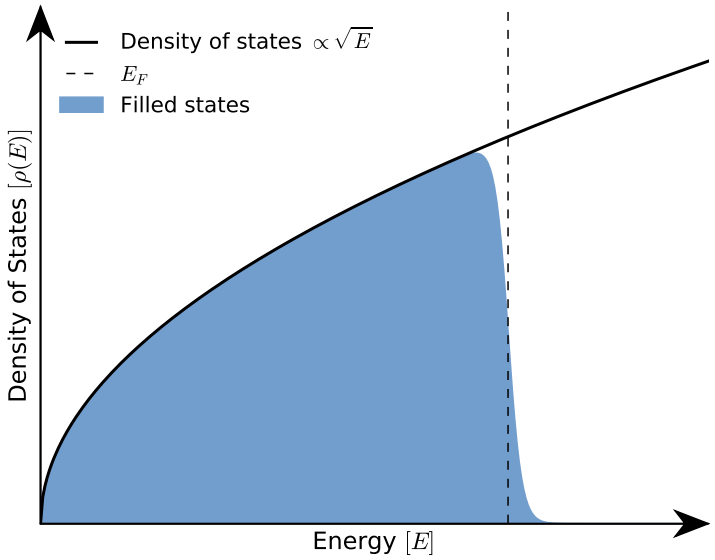

Figure 4.3.: Density of states for a normal metal at $T \neq 0$. The thermal smearing is exaggerated here to be able to see it's form.

Aside

It is important to note that it is only electrons near the surface of the Fermi sea that carry current!

5. Superconductivity

In radio astronomy, superconductors are used to create highly-sensitive receivers and detectors. Many of these receivers take advantage of unique properties of superconductors. It is therefore necessary to briefly cover the basics.

5.1. Introduction

Superconductors have many bizarre macroscopic properties. The two most famous properties are:

1. exactly zero resistance to DC current ($\rho = 0$ for $T < T_C$), and
2. the ejection of magnetic fields ($B = 0$ inside).

Aside

Recall that $\mathbf{B}$ represents the **magnetic field**:

$$\mathbf{B} \equiv \mu_0(\mathbf{H} + \mathbf{M}) \equiv \mu_0\mu_r\mathbf{H} \tag{5.1}$$

In SI units,

$\mathbf{B}$ is measured in Teslas (T)

1 T = 10,000 Gauss (G) = 1 N s $C^{-1}m^{-1}$

The Earth's magnetic field at the surface $\approx$ 0.5 G

$\mathbf{H}$ is the **magnetic field strength** measured in A/m

$\mu_0\mathbf{M}(= \mu_0\chi\mathbf{H})$ is the **magnetisation field** (property of the material)

For superconductors, $\mathbf{B} = 0 \therefore \mathbf{M} = -\mathbf{H}$ meaning that superconductors are perfectly diamagnetic materials. Recall the basic types of magnetic materials:

Paramagnetism Magnetic moments will align with an external field, resulting in an attractive force. The magnetic permeability is greater than 1 ($\mu_r > 1$). Thermal agitation causes the moments to become mis-aligned once the field disappears.

Ferromagnetism Same as paramagnetism except that the magnetic moments will remain aligned after the external magnetic field disappears.

Diamagnetism Magnetic moments will anti-align to external fields, resulting in a repulsive force.

5.1.1. Brief History

1911 While developing new techniques to liquify gasses, Heike Onnes discovers that the resistance of mercury drops to zero when cooled by liquid helium. The resistance is not just small—it is exactly zero!

1933 Meissner and Ochsenfeld discover that magnetic fields are completely expelled from superconductors meaning that they are perfect diamagnets.

1935 Fritz and Heinz London (brothers) develop the first phenomenological theory of superconductivity. Their theory is able to explain the Meissner effect.

1950 Landau and Ginzburg develop their phenomenological theory of superconductivity, which then predicts type-I and type-II superconductors.

1957 Bardeen, Cooper and Schrieffer develop BCS theory (based on the initials of their names), which is a complete microscopic theory of superconductivity. This theory explains how pairs of electrons, called Cooper pairs, are able to form within superconductors, and travel with zero resistance.

1962 Josephson predicts quantum tunnelling of Cooper pairs between two superconductors that are separated by a thin insulator.

5.1.2. Superconducting Materials

Many metals can become superconducting when they are cooled below their critical temperature (T_C), which is a characteristic of the material. Even more can become superconducting when an external pressure is also applied. A full list is given in Figure 5.1. It is interesting to note that the noble metals (gold, silver, copper), which are normally very good conductors, *never* become superconducting no matter the temperature or pressure.

5.2. Characteristics of Superconductors

In superconductors cooled below T_C, interactions between lattice vibrations (phonons) and electrons allow pairs of electrons to form, called **Cooper pairs** (depicted in Figure 5.2[1]). Each pair is composed of two electrons which have opposing momentum and spin. Although this seems counter-intuitive, the Cooper pairs interact over a large enough distance that electromagnetic repulsion is no longer significant, and the phonon interaction is enough to form a weak bond.

I need to clarify:

Does this mean that Cooper pairs are constantly breaking/reforming?

While the constituent electrons are fermions (1/2 spin) that obey Fermi-Dirac statistics and the Pauli exclusion principle, Cooper pairs are quasi-bosons (integer spin), which obey Bose-Einstein statistics. Therefore, all of the Cooper pairs can occupy the same energy level and they can be described by a single wave function:

$$\Psi(\mathbf{r}) = \sqrt{n_s(\mathbf{r})}e^{i\varphi(\mathbf{r})} \tag{5.2}$$

This gives rise to many different macroscopic effects described in the following subsections.

5.2.1. Energy Bandgap

As the temperature drops below T_c in a superconductor, Cooper pairs form at the surface of the Fermi sea. The "depth" of the Fermi sea that condenses into Cooper pairs is governed by the maximum phonon frequency (i.e., the Debye frequency, ω_D) and the Pauli exclusion principle. The binding energy of a Cooper pair will be:

$$\Delta(T=0) = 2\hbar\omega_D \ \exp\left\{\frac{-2}{V_0 \ \rho(E_F)}\right\} \approx 1.76 \ kT_c \tag{5.3}$$

It will then be energetically favourable for all of the electrons within the range $E_F - \Delta < E < E_F + \Delta$ to condense into Cooper pairs. This creates a range of energies within which single, unpaired electrons do not exist. This is often compared to the bandgap seen in superconductors. The density of states ($\rho(E)$) in a superconductor is given by:

$$\rho(E) = \begin{cases} 0 & \text{if } |E| < \Delta \\ N(E_F)\dfrac{|E|}{\sqrt{E^2-\Delta^2}} & \text{if } |E| > \Delta \end{cases} \tag{5.4}$$

The electrons that condense into Cooper pairs are depicted in $\vec{k}$-space in Figure 5.3 and the resultant density of states is shown in Figure 5.4. Note that for $0 < T < T_c$, some of the electrons below the bandgap will be thermally excited above the gap (Figure 5.4b).

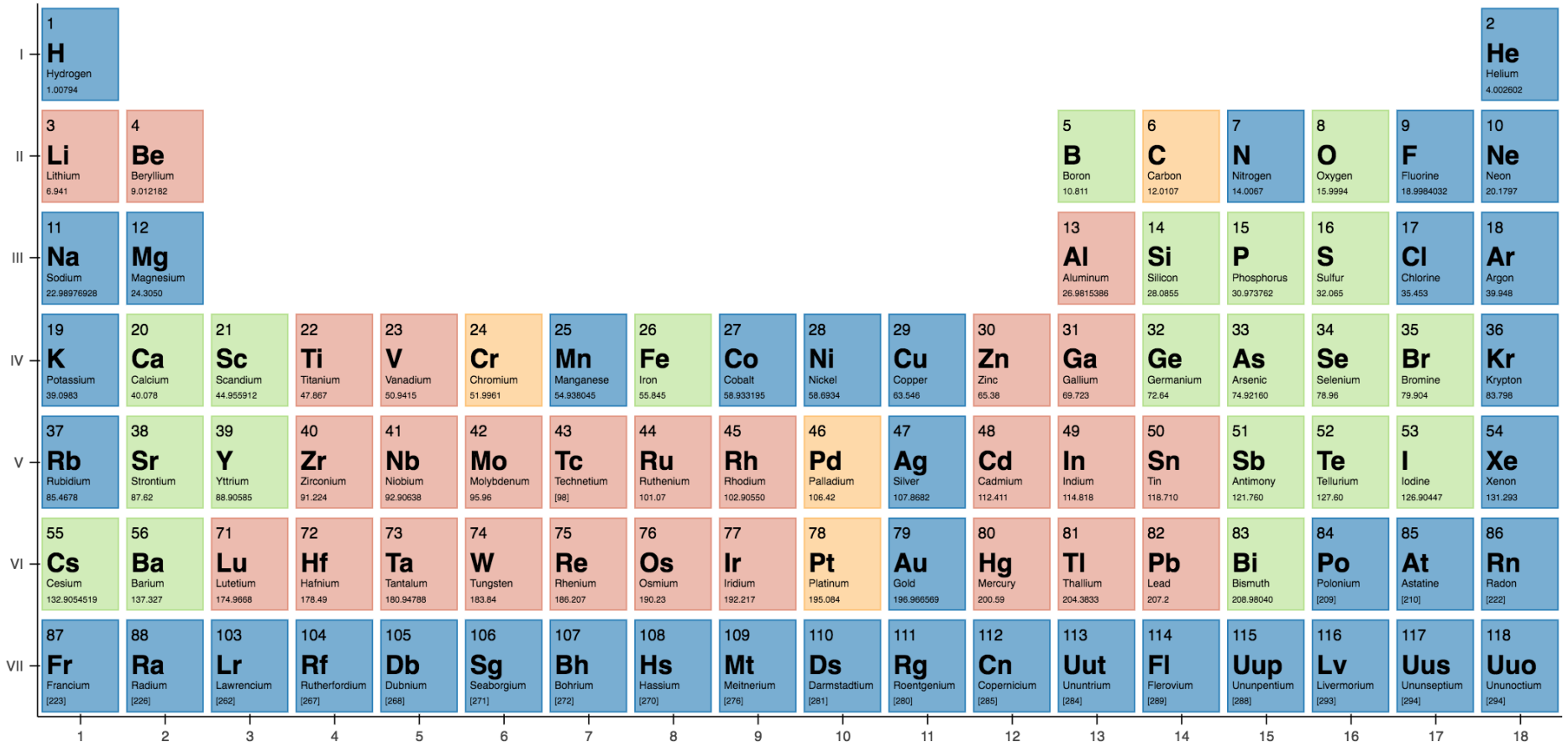

Figure 5.1.: Elements which can become superconducting at ambient pressure are shown in red, those which can under pressure are shown in green, and those which are only superconducting in certain crystal forms are shown in yellow. All others are shown in blue. Note that most elements are type-I superconductors except for niobium, technetium, vanadium, silicon, and some forms of carbon. Plot generated with Bokeh.

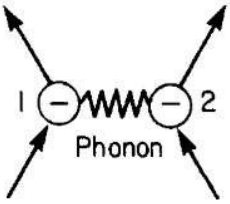

Figure 5.2.: Electron-phonon interaction.

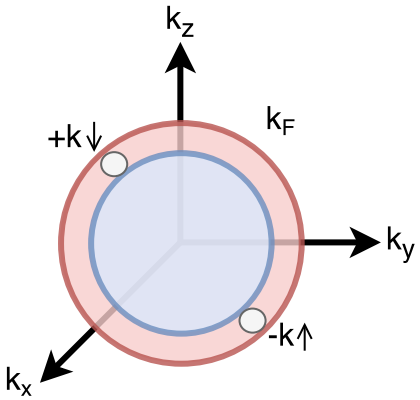

Figure 5.3.: Density of states in k-space. The blue area represents the normal electrons and the red area represents the area that condenses into Cooper pairs.

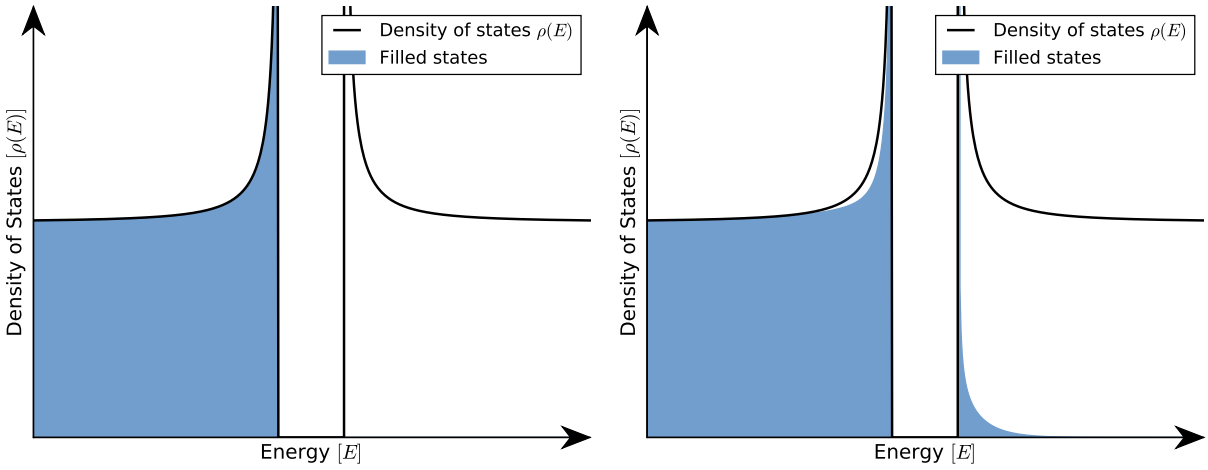

(a) $T = 0$ (b) $T > 0$

Figure 5.4.: Density of states for a superconductor.

I need to clarify:

Why don't the thermally excited electrons create any resistance? Can't they scatter?

5.2.1.1. Expulsion of Magnetic Fields

When electrons condense into Cooper pairs, condensation energy is gained. However, magnetic energy is also required for the expulsion of the magnetic fields. If this magnetic energy exceeds the energy gained through condensation, the superconductor will become partially or totally normal once again. There

[1]Figure from http://what-when-how.com/wp-content/uploads/2011/07/tmp6C341_thumb22.jpg

therefore exists a critical magnetic field (B_c) that if exceeded will cause a superconductor to become normal. This magnetic field limit can also be surpassed by passing a current through the superconductor, which causes the magnetic field at the surface to surpass B_c. As shown in Figure 5.5[2], there are two general classifications of superconductors.

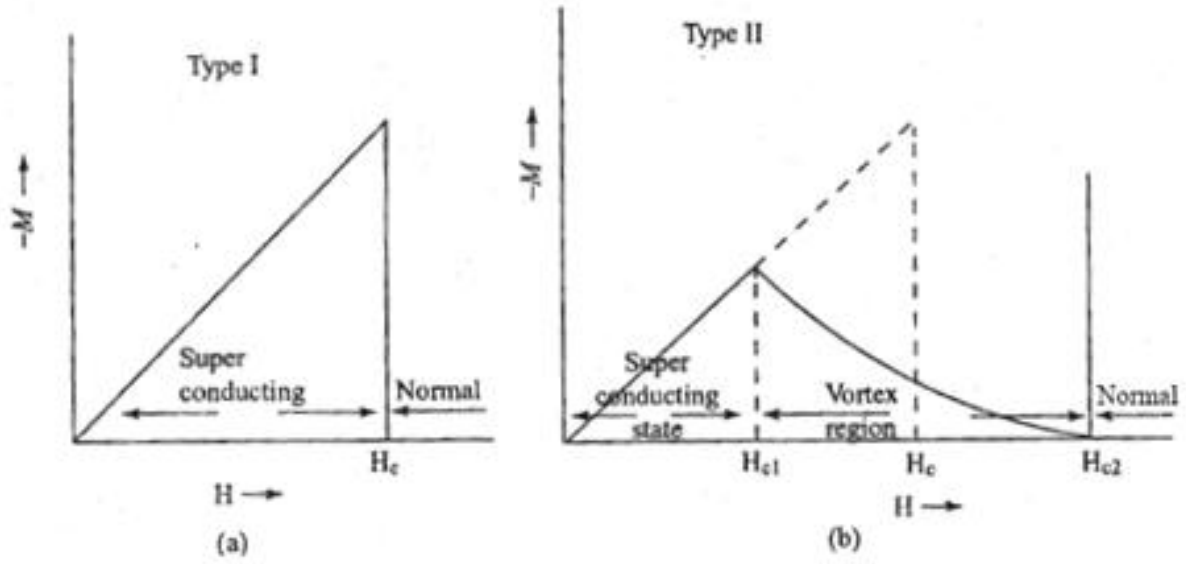

Figure 5.5.: Type I vs Type II superconductors.

5.2.1.2. Type I Superconductors

In a Type I superconductor, the superconductor is a perfect diamagnet ($\mathbf{M} = -\mathbf{H}$) until the critical field is reached after which it becomes a normal metal. Note that the critical field is related to the critical temperature through:

$$B_C = B_0 \left[1 - \left(\frac{T}{T_C}\right)^2\right] \tag{5.5}$$

5.2.1.3. Type II Superconductors

Type II superconductors have the ability to enter a mixed state as shown in Figure 5.5. Below B_{C1}, the superconductor will be a perfect diamagnet (i.e., the same as a Type I superconductor). But between B_{C1} and B_{C2}, magnetic field vortices roughly 100 nm in diameter will form. Each vortex consists of a supercurrent circulating a normal metal thread, and each thread allows a quantised amount of magnetic flux to pass through the superconductor:

$$\Phi_0 = \frac{h}{2e} \sim 2.067 \times 10^{-15} \text{ Wb} \tag{5.6}$$

If a current passes through a superconductor possessing magnetic vortices, the vortices will move along with the current. This movement will dissipate energy causing an effective resistance. To stop the vortices from moving, they must be pinned in place. This is done by introducing inclusions of normal metal[3] within the superconductor. Type II superconductors are used in most practical applications due to their ability to handle much higher magnetic fields and currents than type-I materials.

[2]Figure from http://ffden-2.phys.uaf.edu/webproj/211_fall_2014/Jonah_Jeffries/Jonah_Jeffries/typeonetypetwo.JPG
[3]The normal metals won't affect the resistance of the superconductor.

5.2.2. Penetration Depth

The magnetic field won't be zero at the surface since $-\mathbf{M}$ must be generated by supercurrents within the superconductor. The depth at which B drops to $1/e$ its value at the surface is called the penetration depth (λ) and is a property of the material.

5.2.3. Coherence Length

The distance separating the electrons in Cooper pairs can often be several lattice intervals. This distance is called the coherence length (ξ). The intrinsic coherence length is given by:

$$\xi_0 = \frac{\hbar v_F}{\pi \Delta} \tag{5.7}$$

Aside

To determine the length of lattice that remains distorted after an electron shoots by[a], we can do a back of the envelope calculation using the Debye frequency and the Fermi velocity. The fastest frequency at which the phonons can vibrate is the Debye frequency:

$$\omega_D = \sqrt{\frac{4k}{m_{atom}}} \sim 10^{-13} \text{ s} \tag{5.8}$$

The Fermi velocity (v_F) will be on the order of 10^6 m/s. Therefore the length of distorted lattice is:

$$\frac{v_F}{\omega_D} \sim 100 \text{ nm} \tag{5.9}$$

This is approximately the size of a Cooper pair.

[a] This procedure is taken from http://physics.oregonstate.edu/~minote/COURSES/ph671/lib/exe/fetch.php?media=day12_2013.pdf

6. Quantum Tunnelling

6.1. Introduction

A superconductor–insulator–superconductor (SIS) junction is depicted in Figure 6.1. Electrons can tunnel through the insulator provided that the separation distance is adequately small (i.e., on the order of ∼10 Å). The tunnelling current can take the form of Cooper pair tunnelling (a.k.a., Josephson tunnelling, Section 6.2) or quasi-particle tunnelling (Section 6.3). Note that this is not due to conduction through the insulator or dielectric breakdown—it is a macroscopic, quantum mechanical effect!

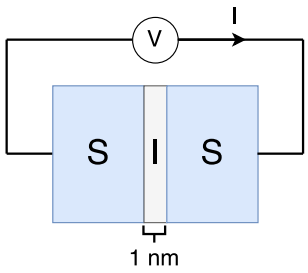

Figure 6.1.: A Josephson junction consists of two superconductors (S) separated by a thin insulator (I). When the junction is used for quasi-particle tunnelling, the junction is typically called an SIS junction.

6.2. Josephson Tunnelling

The basic Josephson tunnelling equations are [7]:

$$V(t) = \frac{\hbar}{2e}\frac{d\varphi}{dt} \tag{6.1a}$$

$$I(t) = I_c \sin(\varphi(t)) \tag{6.1b}$$

where φ is the phase difference of the Cooper pair wavefunctions on either side of the insulator (a.k.a., the Josephson phase), and I_C is the critical current. These equations can be combined to form:

$$I(t) = I_c \sin\left(\varphi_0 + \frac{2e}{\hbar}\int_0^t V(t')dt'\right) \tag{6.2}$$

Aside

The critical current is given by [8]:

$$I_c = \frac{\pi\Delta(T)}{2eR_n} \tanh\left(\frac{\Delta(T)}{2kT}\right) \tag{6.3}$$

At $T = 0$:

$$I_c = \frac{\pi\Delta(0)}{2eR_n} = \frac{\pi}{4}\frac{V_{gap}}{R_n} \tag{6.4}$$

Special cases of Equation 6.2 include:

1. **V = 0:** Even if there is zero voltage across the junction, tunnelling current will still exist and it will take some value $-I_c < I(t) < I_c$. This is called the **DC Josephson effect** and the current is typically called the **supercurrent**.
2. **V = const. ≠ 0:** If the applied voltage has some non-zero, constant value, the Josephson tunnelling current with oscillate with a frequency:

$$\nu = \frac{2e}{h}V \sim 483.6 \text{ GHz per mV} \tag{6.5}$$

   This is called the **AC Josephson effect**, and it has even been used to create integrated, on-chip local-oscillators (e.g., [9]).
3. **V**= $V_0 + V_\omega \cos(\omega t + \theta)$: An AC signal will generate a step structure into the DC I-V curve (called **Shapiro steps**). The full explanation is given in [10].

I need to clarify:

How are Josephson receivers operated? Are they used for mixing?

6.2.0.1. Experimental Josephson Current

Without any microwave field applied, three special areas can be identified on the experimental DC I-V curve of a Josephson junction:

1. At $V = 0$, a spike corresponding to the DC Josephson current will be seen.
2. For low voltages, the AC Josephson effect will be noticeable. Past a certain voltage however, the intrinsic junction capacitance will short-circuit the AC Josephson effect.
3. For a very narrow voltage range, the AC Josephson effect will match the receiver's tuning frequency leading to a small peak. For example, if a mixer is designed for $f_{mixer} = 230$ GHz, a spike at $V = f_{mixer}\hbar/2e = 0.475$ mV will be seen. This is called the **Fiske step**.

In an SIS junction, where only quasi-particle tunnelling is desired, Josephson tunnelling should be suppressed to reduce the resultant shot noise. Since the critical current is strongly affected by a magnetic field applied across the junction,

$$I_c = I_c(0)\left|\frac{J_1(x)}{x}\right| \tag{6.6a}$$

$$x = \frac{\pi\Phi}{\Phi_0} \tag{6.6b}$$

solenoids and permanent magnets are often used to suppress Josephson currents.

6.2.0.2. Josephson Inductance

Josephson junctions can also be used as inductors (some parametric amplifiers rely this effect). Unlike conventional inductors, no magnetic field is generated by the Josephson junction. Instead, the inductance is related to the kinetic inductance of the charge carriers tunnelling through the junction. This inductance is given by:

$$L_J = V\left(\frac{\partial I}{\partial t}\right)^{-1} = \frac{\Phi_0}{2\pi I_c \cos(\varphi_0)} = \frac{L_J(0)}{\cos(\varphi_0)} \tag{6.7}$$

6.3. Quasi-Particle Tunnelling

In an SIS junction (Figure 6.1), the electron wavefunctions on one side of the barrier will have finite probability amplitudes in the opposite superconductor if the separation distance is adequately small. This means that they there is a finite chance that the electrons are able to do a quantum jump across the insulator without losing any energy. Electrons can tunnel across the barrier provided that (a) the new state has the same energy as the original state (conservation of energy), and (b) the new energy state is empty in that superconductor (Pauli exclusion principle). The tunnelling current will then be proportional to the the number of filled states in one metal that are aligned with empty states in the second metal:

$$I(V) \propto \int \{\rho_1 (E-V) f (E-V) \rho_2 (E) [1 - f (E)] - \rho_1 (E-V) [1 - f (E-V)] \rho_2 (E) f (E)\} \, dE \tag{6.8}$$

where ρ is the density of states in a superconductor (from BCS theory [11], Equation 5.4) and f is the Fermi probability of a given state being occupied. The first line in Equation 6.8 corresponds to forward tunnelling (e.g., from S_1 to S_2 in Figure 6.1), and the second line corresponds to reverse tunnelling. This equation essentially convolves the filled states in S_1 with the empty states in S_2 (and vice-versa for current in the opposite direction). For simplicity, Equation 6.8 can be reduced to:

$$I(V) \propto \int \rho_1(E-V)\rho_2(E) \{f(E-V) - f(E)\} \, dE \tag{6.9}$$

As an external voltage is applied to an SIS junction, there will initially be nearly zero current (see Figure 6.2a). This is due to the bandgap of the superconductors (Section 5.2.1). At $V \approx V_{gap}$, the applied potential will be able to overcome the binding energy of the Cooper pairs and a large spike in current will be seen. Above V_{gap}, the junction will take on its normal-state resistance. In an ideal SIS junction, the quasi-particle tunnelling is extremely non-linear.

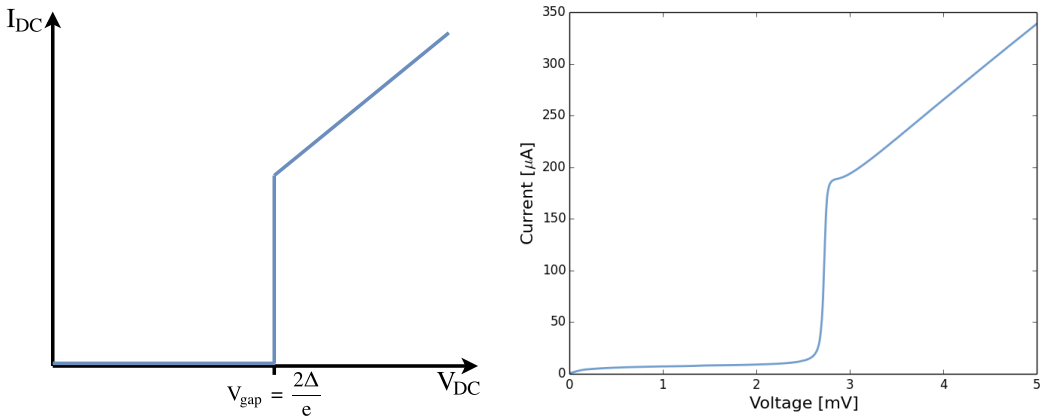

(a) Ideal I-V curve.

(b) Experimental I-V curve.

Figure 6.2.: Quasi-particle tunnelling in an SIS junction.

Quasi-particle tunnelling in SIS junctions was first observed in 1960 by Giaever [12] and Nicol, Shapiro and Smith [13]. Since the gap voltage is related to the binding energy of Cooper pairs, these experiments were a major confirmation of BCS theory[1].

[1] Giaever shared the 1973 Nobel Prize with Josephson (who predicted Josephson currents [7] in 1962) and Esaki (who was the first to show quantum tunnelling in semiconductors [14] in 1957.)

6.3.1. Experimental Quasi-Particle Tunnelling

As seen in Figure 6.2, the experimental I-V curve is not as sharp as the ideal I-V curve. It also has subgap leakage current below V_{gap} and a knee feature is often seen just above the transition voltage. To recreate experimental data, Equation 6.9 can be solved numerically, but several other factors must be included to achieve a close approximation:

1. Realistic SIS junctions have finite temperatures, leading to thermally excited quasi-particles existing above the gap (even below V_{gap}), and therefore sub-gap leakage current (I_{sg}). The number of thermally excited quasi-particles is described by the Fermi function in Equation 6.9. Furthermore, the binding energy is also related to the temperature through:

$$\Delta(T) = \Delta(0)\sqrt{\cos\left[\frac{\pi}{2}\left(\frac{T}{T_c}\right)^2\right]} \tag{6.10}$$

2. Junction defects and the finite quasi-particle lifetimes within the gap will lead to the transition becoming smeared. This can be modelled by adding a small imaginary component to E when solving Equation 5.4 (e.g., the Γ term in [15]), or by adding a small imaginary component to the binding energy (e.g., $\Delta = \Delta_1 - j\Delta_2$, as in [16, 17]).

3. The proximity effect will create a small knee just above the gap. This can be modelled by the recursive equations listed in [18].

Equation 6.9 was used to determine the tunnelling current seen in Figure 6.3. The first 2 factors listed above were included (the proximity effect is not included here). Realistically, Δ_2 will be related to the T as well, but they are isolated here to better see their effect.

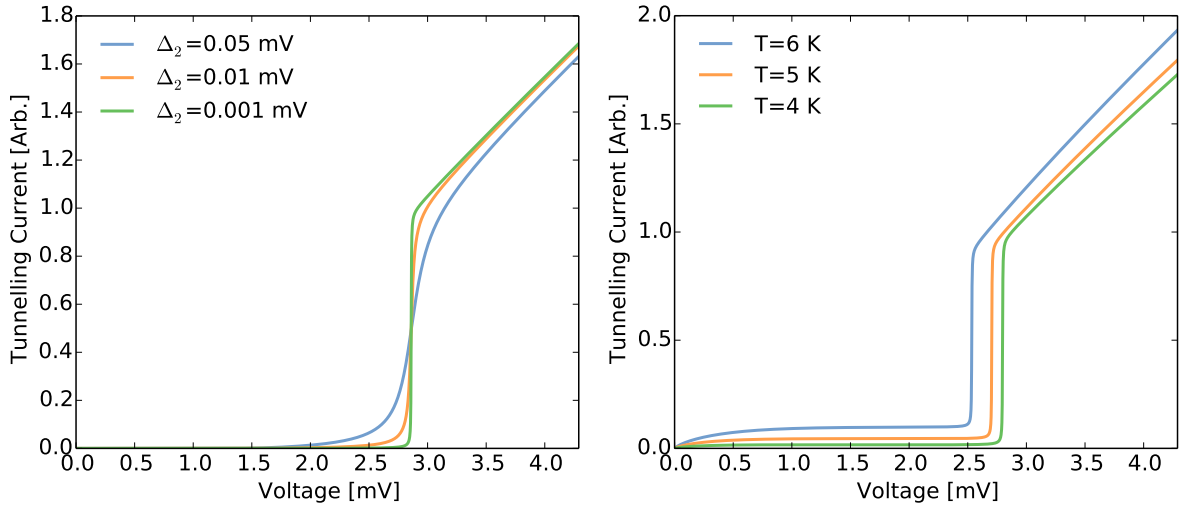

(a) Increasing the imaginary component of the binding energy ($T = 0$) causes the transition to smear.

(b) Increasing the temperature ($\Delta = 0.001$ meV) will raise the subgap current and lower the gap voltage.

Figure 6.3.: Quasi-particle tunnelling current generated numerically from Equation 6.8.

6.3.2. Photon-Assisted Tunnelling

It is possible for quasi-particles below the bandgap to tunnel through the barrier by absorbing the necessary energy from a photon. This was first shown experimentally by Dayem and Martin in 1962 [19] and was then described by Tien in 1963 [20]. The frequency of the photon (ν_γ) must be $> (2\Delta - eV_0)/nh$ where n is the number of absorbed photons. When this is satisfied, **photon-assisted tunnelling** can occur.

As described by Tien [20] and Tucker and Feldman [21], the applied microwave signal (source of the photons) and DC bias can be represented by a combined voltage:

$$V(t) = V_0 + V_\omega \cos(\omega t) \tag{6.11}$$

which has a DC (V_0) and AC ($V_\omega \cos(\omega t)$) component. The DC tunnelling current is then given by:

$$I_0(V_0, V_\omega) = \sum_{n=-\infty}^{\infty} J_n^2(\alpha(V_\omega))\ I_{dc}(V_0 + n\hbar\omega/e) \tag{6.12}$$

where $\alpha = eV_\omega/\hbar\omega$ is the junction drive level. The $J_n^2(\alpha)$ term can be thought of as the probability of a quasi-particle absorbing n photons at a given drive level, α. This will induce a step-like structure into the I-V curve (e.g., Figure 6.4).

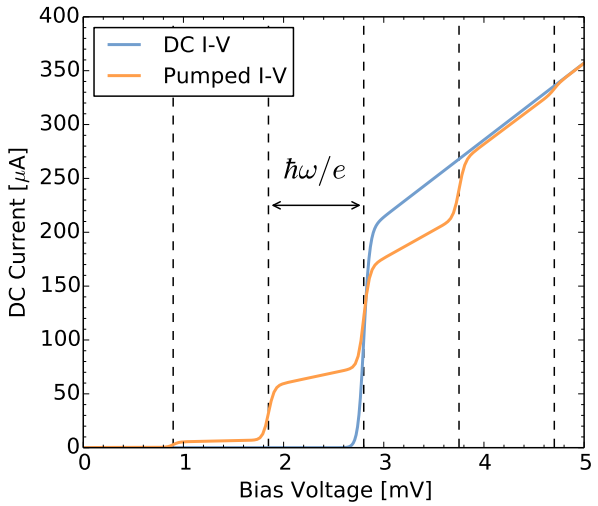

Figure 6.4.: Pumped I-V curve for $\nu = 230$ GHz and $\alpha = 1.2$. The dashed lines mark $V_{gap} \pm nh\nu/e$.

7. SIS Mixer Theory

8. Extra-Galactic Star Formation

- Star formation (SF) is a driving force behind galaxy evolution
  - chemical enrichment
  - heating the ISM
  - (indirectly) production of dust through the winds of dying stars
- SF is a complex process (e.g., gas accretion → cooling → collapse → stellar birth)
  - scaling laws describe correlations between global properties
  - not many apply to cold gas
  - Schmidt-Kennicutt (SK) laws
    - $\Sigma_{\rm SFR} \propto \Sigma_{\rm gas}^{\alpha}$
    - Schmidt 1959, Kennicutt 1998*, Kennicutt and Evans 2012
- Peak of star formation from z=1-3
  - Dominated by dusty galaxies:
    - Luminous Infrared Galaxies (LIRGs, $L_{IR} = 10^{11} - -10^{12}\ L_{\odot}$)
    - Ultra Luminous Infrared Galaxies (ULIRGs, $L_{IR} > 10^{12}\ L_{\odot}$)
  - L_{IR} is an ideal tracer of SFR for dusty galaxies
    - Assume that dust is heated by star formation
  - CO traces H_2
    - Bolatto 2013
- Galaxy main sequence
  - tight relationship between SFR and stellar mass
  - if SFR is higher than normal rate for a given stellar mass → starburst
    - likely driven by a recent merger
  - Distinction between main sequence and starburst galaxies can also be determined by comparing L_{IR} and L'_{CO}
    - If L_{IR} is higher than normal for a given L'_{CO} → starburst
    - merger funneling gas towards the inner regions of a galaxy
    - α_{CO} depends on whether a galaxy is in starburst mode
- Some LIRGs/ULIRGs show signs that they have an AGN at the center
  - classical picture of starburst: major merger → AGN phase
  - AGN: heating the dust, expelling the gas, quenching star formation through feedback mechanisms
  - star forming galaxies have prominent PAH features from photodissociation regions (PDRs)
    - AGN can dilute these features
    - AGN emission can head the dust in the ISM to >100 K producing a significant contribution to the far IR emission

- Scatter between L_{IR} and L'_{CO}
  - AGN contribution to L_{IR}

8.1. Star formation studies

1. Kirkpatrick 2014 (LMT, [22])
   - ΛCDM: $H_0 = 71$ km s^{-1} Mpc^{-1}, $\Omega_m = 0.27$, $\Omega_A = 0.73$
   - Sample: 24 galaxies
     - chosen based on PAH equivalent widths (EW) and L_{IR} for $\tau < 90$ min
     - $z = 0.04 - 0.36$ and $L_{IR} = 1.8 \times 10^{10} - 1.3 \times 10^{12}$ $L_\odot$
   - CO observations:
     - Large Millimetre Telescope (LMT)
       - Volcan Sierra Negra, Mexico (4600 m)
       - 50 m dish, only 32.5 m was operational in early science phase, active surface
       - sensitivity 7.0 Jy/K at 3 mm
       - Redshift Search Receiver, 73–111 GHz simultaneous bandwidth
     - $>3\sigma$ detection on 17/24 galaxies
     - no correlation between σ_{rms} and S/N
     - data analyzed using DREAMPY
     - no aperture corrections needed
   - L_{IR}
     - $L_{IR}(5 - 1000\mu\text{m})$ from Wu [23]
     - Converted to $L_{IR}(8 - 1000\mu\text{m})$ by multiplying by 0.948
     - Corrected for different cosmologies by multiplying by 0.970
     - AGN identified by fitting SED models
   - SFR
     - masses from Shi [24]
2. Wu 2010 (5MUSES analysis, [23])
   - ΛCDM: $H_0 = 70$ km s^{-1} Mpc^{-1}, $\Omega_m = 0.27$, $\Omega_A = 0.73$
3. Saintonge 2011 (COLD GASS, [25])
   - ΛCDM: $H_0 = 70$ km s^{-1} Mpc^{-1}

8.2. Galaxies

The Hubble sequence was originally designed to classify the shape/morphology of galaxies (Figure 8.1); however, it also represents a range of young stellar content and star formation activity. The difference in appearance between elliptical (E) galaxies and spiral (S) galaxies is a result of the initial star formation rate. In general,

- **elliptical galaxies** collapsed and formed stars quickly, and
  - The collapse uses up the gas very quickly. They have a **red appearance** because only the **old stars** are still alive.

- **spiral galaxies** formed stars much slower but at a sustained rate.
  - The **central area** is red due to a high population of **old stars**, while the **arms** are blue due to **active star formation and young stars.**

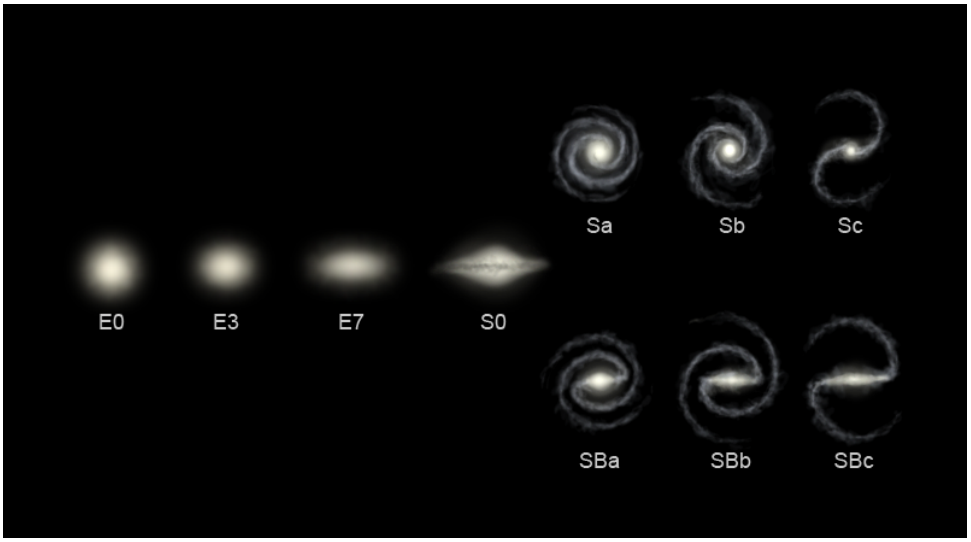

Figure 8.1.: Hubble sequence

8.3. The Interstellar Medium

Within galaxies, the matter that exists in between stars is called the **interstellar medium (ISM)**. By mass, the ISM is **∼99% gas and ∼1% dust**. Of the gas, **∼70% is H_2, ∼28% is He, and ∼1.5% consists of other elements and molecules**, again by mass [26]. The hydrogen to helium ratio is the result of primordial nucleosynthesis[1], while the other molecules result from stellar evolution. Gas in the ISM exists in three phases:

1. **Ionised gas** ($> 10^4$ K), which is gas heated by supernovas shock waves. It is seen through H_α, FIR, and X-ray observations.

2. **Atomic gas** (∼100–1000 K), which includes warm atomic gas (∼1,000 K) in filaments and cold atomic gas (∼100 K) in clouds. It is observed through the 21 cm line, which is the result of a transition between two hyperfine energy levels in neutral hydrogen.

3. **Molecular gas**, which is the coldest form of gas. In large, dense clouds of molecular gas, stars can form!

8.3.1. Molecular Clouds

All stars are born in enormous clouds of molecular gas and dust. These clouds can be up to $\sim 10^6$ $M_\odot$ in mass and 100 pc in diameter. Their structure is inhomogenous with clumps and cores of increased density forming within the clouds (see Table 8.1). Because of the dust, visible light cannot see into these clouds. Instead, infrared and millimetre-wave observations must be used.

[1] Fusion during the big bang.

Table 8.1.: Physical properties of interstellar clouds (reproduced from [27])

	Giant Molecular Cloud Complex	Molecular Cloud	Star-Forming Clump	Protostellar Core
Size (pc)	10–60	2–20	0.1–2	$\lesssim 0.1$
Density[a] ($n(H_2)/cm^3$)	100–500	10^2–10^4	10^3–10^5	$> 10^5$
Mass ($M_\odot$)	10^4–10^6	10^2–10^4	10–10^3	0.1–10
Temperature (K)	7–15	10–30	10–30	7–15

[a]Compare this to sea level on Earth where the density of molecules is $\sim 10^{19}/cm^3$.

8.4. Star Formation

Stars form in the densest regions of molecular clouds (a.k.a., protostellar cores, as in Table 8.1). The gas is only able to collapse under gravity and form a protostar if it is very cold. Atomic gas is not able to get to temperatures sufficiently low because it does not emit efficiently at low temperatures. Only molecular gas is able to cool to temperatures below 100 K.

8.4.1. Empirical Star Formation Laws

Scaling relations describe the connection between the star formation rate (SFR) and the global properties of the gas (e.g., gas density, temperature, metallicity, etc.).

Star formation rate (stars formed per unit time per unit area (in a disc)):

$$\dot{\Sigma}_\star = \dot{M}_\star/\text{area} \tag{8.1}$$

Gas consumption timescale:

$$\tau_{SF} \equiv \Sigma_{gas}/\dot{\Sigma}_\star \tag{8.2}$$

Kennicutt-Schmidt law [28]:

$$\dot{\Sigma}_\star \approx 2.5 \times 10^{-4} \left(\frac{\Sigma_{gas}}{M_\odot \text{ pc}^{-2}}\right)^{1.4} M_\odot \text{ yr}^{-1} \text{ kpc}^{-2} \tag{8.3}$$

where $\Sigma_{gas} = \Sigma_{HI} + \Sigma_{H_2}$

Local star formation, the Schmidt law:

$$\dot{\Sigma}_\star \approx 7 \times 10^{-4} \left(\frac{\Sigma_{H_2}}{M_\odot \text{ pc}^{-2}}\right)^{1.0\pm0.2} M_\odot \text{ yr}^{-1} \text{ kpc}^{-2} \tag{8.4}$$

8.4.2. Star Formation Diagnostics

UV Continuum (1250–2500 Å): The number of massive stars is proportional to SFR.

$$\frac{\dot{M}_\star}{M_\odot \text{ yr}^{-1}} \approx 1.4 \times 10^{-28} \left(\frac{L_{UV}}{\text{erg s}^{-1} \text{ Hz}^{-1}}\right) \tag{8.5}$$

Nebular emission lines : The ISM around young, massive stars is ionised by Lyman continuum photons produced by these stars, giving rise to HII regions.

$$\frac{\dot{M}_\star}{M_\odot \text{ yr}^{-1}} \approx 7.9 \times 10^{-42} \left(\frac{L_{H\alpha}}{\text{erg s}^{-1}}\right) \tag{8.6}$$

Forbidden lines :

$$\frac{\dot{M}_\star}{\mathrm{M}_\odot\ \mathrm{yr}^{-1}} \approx 1.4 \times 10^{-41}\ \left(\frac{L_{\mathrm{OII}}}{\mathrm{erg\ s}^{-1}}\right) \tag{8.7}$$

FIR continuum : UV photons are absorbed by dust in the ISM surrounding young stars, which is then re-emitted in the far-infrared (FIR).

$$\frac{\dot{M}_\star}{\mathrm{M}_\odot\ \mathrm{yr}^{-1}} \approx 4.5 \times 10^{-44}\ \left(\frac{L_{\mathrm{FIR}}}{\mathrm{erg\ s}^{-1}}\right) \tag{8.8}$$

8.5. Exploring Scaling Relations Across Cosmic Time

8.5.1. Target Galaxies

- 19 galaxies from 5MUSES
  - ⋆ $0.025 \leq z \leq 0.205$, $\langle z \rangle = 0.101$
  - ⋆ 109.2 MPc $\leq D_L \leq$ 1012.1 MPc, $\langle D_L \rangle = 469.3$ MPc

8.5.2. Molecular Gas Data

8.5.2.1. Observing Strategy at IRAM 30 m

- Target: CO(1–0) line ($\nu_{rest} = 115.271$ GHz), redshifted to ∼105 GHz
- Receivers
  - Frontend: E090
  - Backend: WILMA
    - 2 MHz resolution
- Observed in two runs (June and September)
- Average galaxy requiring 3.5 hrs of integration time for S/N>5 detection

8.5.2.2. Data Analysis

The process that I used to analyse the CO data is summarised below. This is similar to the process used by the COLD GASS survey [25], which was also done at IRAM 30 m.

1. The spectral data was analysed using **IRAM's CLASS software** [29]:
   a) All of the scans were plotted together (using the `plot /index` function) to identify and drop bad data (done by eye).
   b) The scans were averaged together (weighted by $\Delta t \Delta\nu / T_{sys}^2$) to determine the combined spectrum.
      - It would be better to weight by $1/\sigma_{rms}^2$ but I haven't been able to get this option to work.
      - Plotted as velocity (km/s) vs. temperature (K). Axis labels aren't always included on CLASS plots.
   c) The spectrum was smoothed by combining 16 consecutive frequency bins into a single data point (by using 4 consecutive `smooth` function calls)
   d) The baseline was removed by fitting a 1st order polynomial to the data (`base 1`) and then subtracting the line from the spectrum
      - Peaks were ignored (using the `window` function)
      - From this fitting, the baseline RMS error was found (σ_{rms}).
   e) A Gaussian curve was then fitted to the spectral data (using the `line 1` function).
      - Peak should be at:
      $$\nu_{obs} = \frac{115.271 \text{ GHz}}{1+z} \tag{8.9}$$
      - From this fitting, 7 results were output from CLASS:
        - Gaussian curve **area** and its **error** in [K km/s] → S'_{CO}
        - Gaussian curve **position** and its **error** in [km/s]

- Gaussian curve **width**[2] and its **error** in [km/s]
- Gaussian curve **peak** in [K]

- 3 spectra had no obvious peaks, so no Gaussian curve was fit

2. **Integrated line flux** (S_{CO}, [Jy km/s]) was found from the Gaussian curve area (S'_{CO}, [K km/s]).
   - This conversion is specific to IRAM 30m (see [30]):
     - $\frac{S}{T_A^*} \approx 3.906 \frac{F_{eff}}{A_{eff}} \approx 6.2$ Jy/K at 100 GHz, then:

$$S_{CO}\ [\text{Jy km s}^{-1}] \approx 6.2 \cdot S'_{CO}\ [\text{K km s}^{-1}] \tag{8.10}$$

   - The **measurement error** of S'_{CO} (ϵ_{obs}, [K km/s]) can be found from (same as [25] uses):

$$\epsilon_{obs} = \frac{\sigma_{rms} W_{50,CO}}{\sqrt{W_{50,CO}/\Delta\omega_{ch}^{-1}}} \tag{8.11}$$

     where $\Delta\omega_{ch}$ is the width of each channel in [km s^{-1}], and $W_{50,CO}$ is the FWHM of the fitted Gaussian curve.
   - The **signal-to-noise ratio** (SNR or S/N) is then:

$$\text{SNR} = \frac{S}{N} = \frac{S'_{CO,obs}}{\epsilon_{obs}} \tag{8.12}$$

   - If no spectral line was found (i.e., **non-detections**), the upper limit of S_{CO} was found by taking the baseline rms (σ_{rms}), assuming FWHM = 400 km s^{-1}, and then setting S/N = 5.

3. **CO line luminosity** (in units K km s^{-1} pc^2) [31, 32]:

$$L'_{CO} = 3.25 \times 10^7 \cdot S_{CO} \cdot \frac{D_L^2}{\nu_{obs}^2 (1+z)^3} \tag{8.13}$$

   where D_L is the luminosity distance[3] (in units MPc), ν_{obs} is the observed frequency (units GHz), and z is redshift.
   - Note: $L'_{CO} \propto T_b$

4. **Molecular hydrogen mass** (M_{H_2}, in units M$_\odot$):

$$M(\text{H}_2) = \alpha_{CO} \cdot L'_{CO} \tag{8.14}$$

   where $\alpha_{CO} = 3.2$ M$_\odot$ (K km s^{-1} pc^2)$^{-1}$ (value taken from [25]).

8.5.3. IR Data

- Data from 5MUSES. Values taken from (Wu et al. 2010) [23].
  - Gives $L_{IR}(5 - 1000\mu\text{m})$
    - Multiply value by 0.948 to get $L_{IR}(8 - 1000\mu\text{m})$
  - Assume AGN dominated if $EW_{6.2} \leq 0.2$ μm according to (Magdis et al. 2013) [33].

8.5.4. Stellar Masses

Taken from Shi [24].

[2]This width is given as $2 \cdot \sigma$. The FWHM can then be found from:

$$\text{FWHM} = 2\sqrt{2 \ln 2}\ \sigma \simeq 2.355\ \sigma$$

[3]Using a ΛCDM model with $H_0 = 70$ km s^{-1} MPc^{-1} and $\Omega_m = 0.27$ to be consistent with 5MUSES data.

8.5.5. Combined Data

1. **Star formation efficiency** (SFE):

$$SFE = \frac{L_{IR}}{L_{CO}} \tag{8.15}$$

2. **Specific star formation rate** ($sSFR$):

$$sSFR = \frac{SFR}{M^*} \tag{8.16}$$

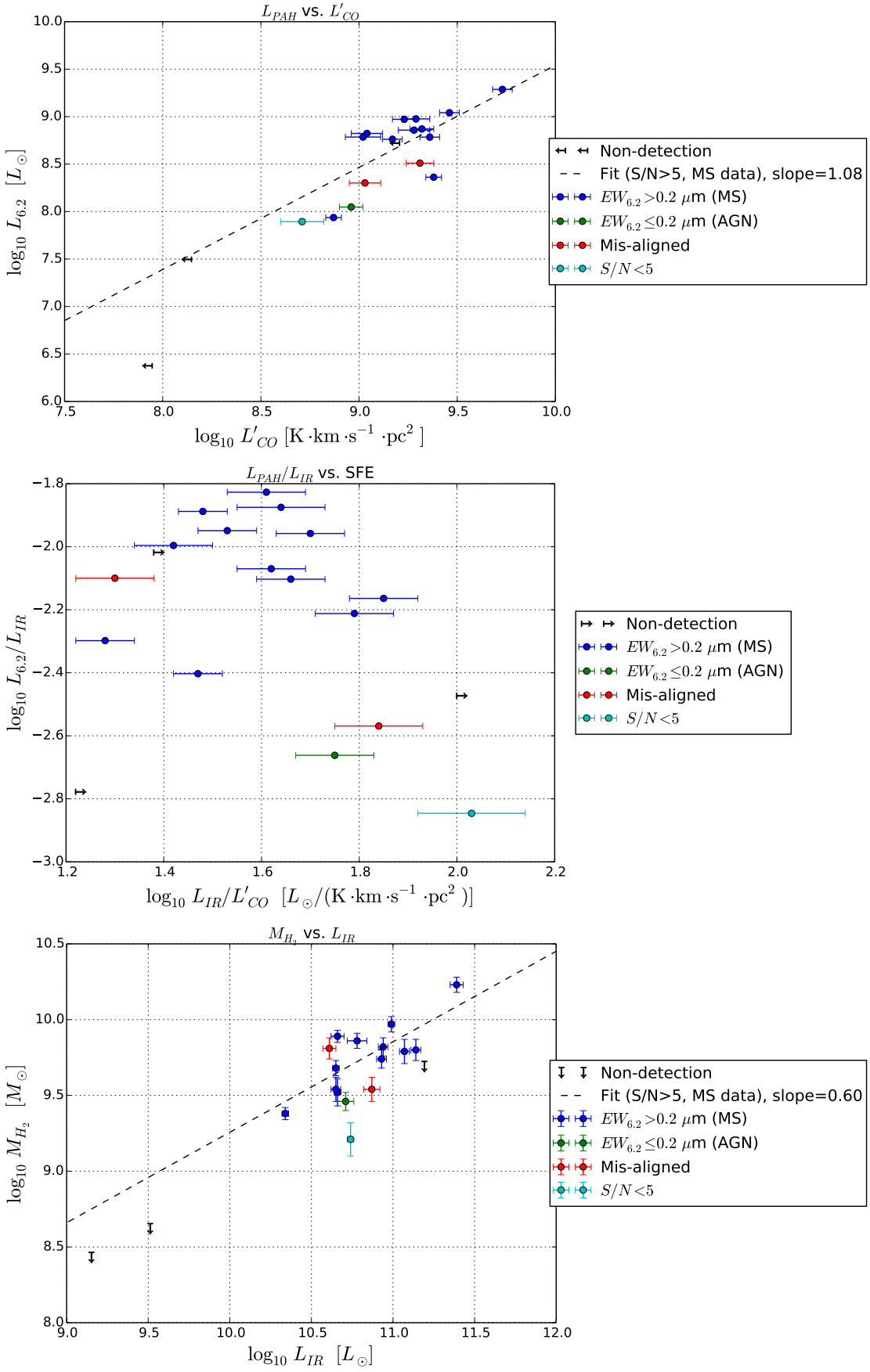

Figure 8.2.: Results

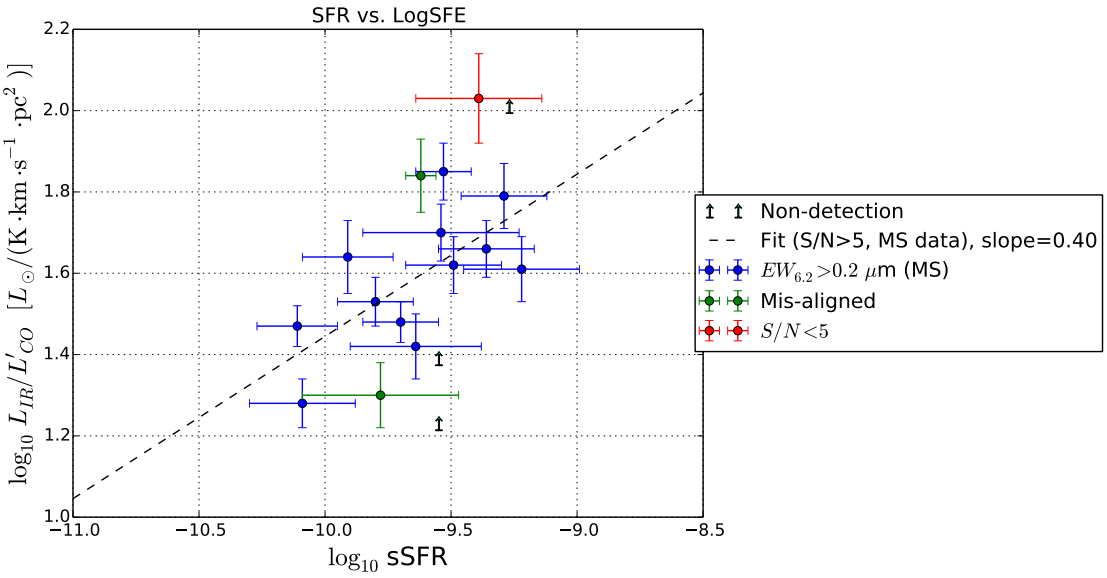

Figure 8.3.: Results

Acknowledgements

In writing this section, I used lecture notes from Professor Dimitra Rigopoulou at the University of Oxford.

A. A Brief History of Radio Astronomy

A brief history of everything leading up to "professional" radio astronomy is included below. Note that many of the dates are approximate.

1666 Isaac Newton discovers that white light is composed of a spectrum of colours, and prisms are able to separate these colours through dispersion.

- Prisms had already been investigated for a long time, but it had previously been thought that the colours were due to some property of the glass (not due to dispersion).
- Note: Dispersion just means that the properties of the glass (e.g., the index of refraction) are frequency dependent, so some colours will bend more than others.

1800 William Herschel discovers infrared light.

- He did this by shining sunlight through a prism, and then placing thermometers under a few of the colours to figure out their relative powers. He then placed one just beyond red (where no light was seen) and discovered that a considerably amount of power was there that human eyes could not detect.
- Herschel was from a very wealthy family. He built some of the most advanced telescopes of his time with his wealth, which helped him discover Uranus.

1873 James Clerk Maxwell publishes "A Treatise on Electricity and Magnetism," and unites electricity and magnetism into a common theory:

$$\nabla \cdot \mathbf{E} = \frac{\rho}{\epsilon_0} \tag{A.1}$$

$$\nabla \cdot \mathbf{B} = 0 \tag{A.2}$$

$$\nabla \times \mathbf{E} = \frac{-\partial \mathbf{E}}{\partial t} \tag{A.3}$$

$$\nabla \times \mathbf{B} = \mu_0 \mathbf{J} + \frac{1}{c^2} \frac{\partial \mathbf{E}}{\partial t} \tag{A.4}$$

- This is still the foundation of all electromagnetics (including the radio-frequency engineering used to design modern radio telescopes).
- He also proved that Saturn's rings had to be made up of dust (not boulders), that the human eye can only sense three colours (red, green and blue), and he produced the first colour photographs.

1888 Heinrich Hertz proves Maxwell's equations by creating the first wireless transmission system using a spark-gap.

- He said that his system had a "purely theoretical interest and no practical interest at all."

1901 Marconi creates the first transatlantic communication system at 500 kHz.

- This system linked Cornwall to Newfoundland, Canada.

1933 Karl Jansky discovers radio emission from the centre of the Milky Way.

- At the time, he was working for Bell Labs and investigating sources of radio noise. He had a system called the "merry-go-round" that could be spun around to investigate where noise was coming from. Most of the noise was from lightening or the spark plugs in cars, but a small amount seemed to come from the sky and repeat every 23 hours and 56 minutes. This was then shown to come from the centre of the Milky Way. This was initially dismissed by the science community. He asked for money to build a purpose-built radio telescope, but was denied funding.

1937 Grote Reber, an amateur radio astronomer, builds the first radio telescope in his backyard.

- He built a 9 m parabolic dish operating at 160 MHz. He was inspired by Jansky, but Bell Labs wasn't hiring during the depression. He discovered non-thermal emission, but synchrotron radiation wasn't explained until the 1950's. He was the only radio astronomer for almost a decade.

1939 World War II pushes many advances in EM instrumentation.

- German U-Boats were devastating transatlantic supply lines. The Tizard Mission was created by the UK to secure manufacturing in the US, but involved the UK sharing many scientific discoveries and blueprints. This included the blueprints for new magnetrons. These new magnetrons were able to create microwave signals powerful enough to make radar feasible. With new magnetron-based radar systems, planes were able to track German U-Boats by bouncing radar off of their periscopes.
- Although a lot of the technology already existed, things like waveguides, horn antennas, reflectors, and antenna arrays were perfected in WWII.

1951 Ewan and Purcell discover the 21 cm line.

- This line had been predicted just a few years earlier, in 1944, by H.C. van de Hulst (one of Oort's students).

1964 Penzias and Wilson discover the CMB.

- They famously thought that the noise was coming from pigeon faeces in the horn reflector, but the noise persisted after all the pigeons had been shot.

Everything after the 1950's is in the era of professional radio astronomy. The Lovell telescope was built in 1957, the VLA in 1973, and the GBT in 1991.

B. Basic Statistics

B.1. Discrete Probability

$N(j)$ is a **discrete distribution**. The total number of items is then:

$$N = \sum_{j=0}^{\infty} N(j) \tag{B.1}$$

The probability of finding a value at j is then:

$$P(j) = \frac{N(j)}{N} \tag{B.2}$$

where $P(j)$ is the **probability density function**. It must be normalised such that:

$$\sum_{j=0}^{\infty} P(j) = 1 \tag{B.3}$$

The **expected value** or **average value** is:

$$\langle j \rangle = \frac{\sum jN(j)}{N} = \sum_{j=0}^{\infty} jP(j) \tag{B.4}$$

The average of the squares is:

$$\langle j^2 \rangle = \sum_{j=0}^{\infty} j^2 P(j) \tag{B.5}$$

The average of some function $f(j)$ is:

$$\langle f(j) \rangle = \sum_{j=0}^{\infty} f(j)P(j) \tag{B.6}$$

The difference from the mean can be written as:

$$\Delta j = j - \langle j \rangle \tag{B.7}$$

The **variance** (σ^2):

$$\sigma^2 \equiv \langle (\Delta j)^2 \rangle \tag{B.8}$$

The **standard deviation** (σ):

$$\sigma = \sqrt{\langle j^2 \rangle - \langle j \rangle^2} \tag{B.9}$$

B.2. Continuous Probability

$\rho(x)$ is the **probability density function**. It represents the odd that at any given time, the function $x(t)$ falls somewhere in the intermal $x \pm \frac{1}{2}dx$. Or more generally, to determine the probability of finding $x(t)$ between a and b:

$$P_{ab} = \int_a^b \rho(x)\ dx \tag{B.10}$$

$\rho(x)$ must be normalised such that:

$$\int_{-\infty}^{+\infty} \rho(x)\ dx = 1 \tag{B.11}$$

The **expected value** $E\{x\}$ or **mean value** $\langle x \rangle$ is:

$$\langle x \rangle = \mu = \int_{-\infty}^{+\infty} x\rho(x)\ dx \tag{B.12}$$

Variance:

$$\sigma^2 = \langle x^2 \rangle - \langle x \rangle^2 \tag{B.13}$$

B.2.1. Gaussian Distribution

A common type of continuous distribution is called a **Gaussian distribution**

$$\rho(x) = \frac{1}{\sigma\sqrt{2\pi}} \exp\left\{-\frac{(x - \langle x \rangle)^2}{2\sigma^2}\right\} \tag{B.14}$$

Bibliography

[1] J. Zmuidzinas and P. Richards, "Superconducting detectors and mixers for millimeter and submillimeter astrophysics," *Proc. IEEE*, vol. 92, no. 10, pp. 1597–1616, oct 2004.

[2] T. L. Wilson, "Techniques of Radio Astronomy," in *Planets, Stars Stellar Syst.* Dordrecht: Springer Netherlands, nov 2013, no. 2001, pp. 283–323. [Online]. Available: http://arxiv.org/abs/1111.1183http://link.springer.com/10.1007/978-94-007-5618-2{_}6

[3] NRAO, "Brightness and Flux Density." [Online]. Available: http://www.cv.nrao.edu/course/astr534/Brightness.html

[4] T. Wilson, K. Rohlfs, and S. Huttemeister, *Tools of Radio Astronomy*, ser. Astronomy and Astrophysics Library. Berlin, Heidelberg: Springer Berlin Heidelberg, 2009. [Online]. Available: http://link.springer.com/10.1007/978-3-540-85122-6

[5] NRAO, "Radiometers." [Online]. Available: http://www.cv.nrao.edu/course/astr534/Radiometers.html

[6] D. Griffiths, *Introduction to Quantum Mechanics*, 2nd ed. Essex: Pearson Education Ltd., 2013.

[7] B. Josephson, "Possible new effects in superconductive tunnelling," *Phys. Lett.*, vol. 1, no. 7, pp. 251–253, jul 1962.

[8] N. R. Werthamer, "Nonlinear Self-Coupling of Josephson Radiation in Superconducting Tunnel Junctions," *Phys. Rev.*, vol. 147, no. 1, pp. 255–263, jul 1966.

[9] V. Koshelets, A. Shchukin, S. Shitov, and L. Filippenko, "Superconducting millimeter wave oscillators and SIS mixers integrated on a chip," *IEEE Trans. Appiled Supercond.*, vol. 3, no. 1, pp. 2524–2527, mar 1993.

[10] M. Cyrot and D. Pavuna, *Introduction To Superconductivity And High-Tc Materials.* Singapore: World Scientific Publishing Co. Pte. Ltd., 1992.

[11] J. Bardeen, L. N. Cooper, and J. R. Schrieffer, "Theory of Superconductivity," *Phys. Rev.*, vol. 108, no. 5, pp. 1175–1204, dec 1957.

[12] I. Giaever, "Electron tunneling between two superconductors," *Phys. Rev. Lett.*, vol. 5, no. 10, pp. 464–466, 1960.

[13] J. Nicol, S. Shapiro, and P. H. Smith, "Direct measurement of the superconducting energy gap," *Phys. Rev. Lett.*, vol. 5, no. 10, pp. 461–464, 1960.

[14] L. Esaki, "New Phenomenon in Narrow Germanium p-n Junctions," *Phys. Rev.*, vol. 109, no. 2, pp. 603–604, jan 1958.

[15] R. C. Dynes, V. Narayanamurti, and J. P. Garno, "Direct Measurement of Quasiparticle-Lifetime Broadening in a Strong-Coupled Superconductor," *Phys. Rev. Lett.*, vol. 41, no. 21, pp. 1509–1512, nov 1978.

[16] T. Noguchi, T. Suzuki, A. Endo, and T. Tamura, "Contribution of the imaginary part of the superconducting gap energy on the SIS tunneling current," *Phys. C Supercond.*, vol. 469, no. 15-20, pp. 1585–1588, oct 2009.

[17] T. Noguchi, T. Suzuki, and T. Tamura, "Subgap Tunneling Current at Low Temperature in Nb/Al-AlN/Nb SIS Junctions," *IEEE Trans. Appl. Supercond.*, vol. 21, no. 3, pp. 756–759, jun 2011.

[18] W. L. McMillan, "Tunneling model of the superconducting proximity effect," *Phys. Rev.*, vol. 175, no. 2, pp. 537–542, 1968.

[19] A. H. Dayem and R. J. Martin, "Quantum interaction of microwave radiation with tunneling between superconductors," *Phys. Rev. Lett.*, vol. 8, no. 6, pp. 246–248, 1962.

[20] P. K. Tien and J. P. Gordon, "Multiphoton process observed in the interaction of microwave fields with the tunneling between superconductor films," *Phys. Rev.*, vol. 129, no. 2, pp. 647–651, 1963.

[21] J. R. Tucker and M. J. Feldman, "Quantum detection at millimeter wavelengths," *Rev. Mod. Phys.*, vol. 57, no. 4, pp. 1055–1113, 1985.

[22] A. Kirkpatrick, A. Pope, I. Aretxaga, L. Armus, D. Calzetti, G. Helou, A. Montaña, G. Narayanan, F. P. Schloerb, Y. Shi, O. Vega, and M. S. Yun, "EARLY SCIENCE WITH THE LARGE MILLIMETER TELESCOPE: EXPLORING THE EFFECT OF AGN ACTIVITY ON THE RELATIONSHIPS BETWEEN MOLECULAR GAS, DUST, AND STAR FORMATION," *Astrophys. J.*, vol. 796, no. 2, p. 135, nov 2014.

[23] Y. Wu, G. Helou, L. Armus, D. Cormier, Y. Shi, D. Dale, K. Dasyra, J. D. Smith, C. Papovich, B. Draine, N. Rahman, S. Stierwalt, D. Fadda, G. Lagache, and E. L. Wright, "INFRARED LUMINOSITIES AND AROMATIC FEATURES IN THE 24 μm FLUX-LIMITED SAMPLE OF 5MUSES," *Astrophys. J.*, vol. 723, no. 1, pp. 895–914, nov 2010.

[24] Y. Shi, G. Helou, L. Yan, L. Armus, Y. Wu, C. Papovich, and S. Stierwalt, "EXTENDED SCHMIDT LAW: ROLE OF EXISTING STARS IN CURRENT STAR FORMATION," *Astrophys. J.*, vol. 733, no. 2, p. 87, jun 2011.

[25] A. Saintonge, G. Kauffmann, J. Wang, C. Kramer, L. J. Tacconi, C. Buchbender, B. Catinella, J. Graciá-Carpio, L. Cortese, S. Fabello, J. Fu, R. Genzel, R. Giovanelli, Q. Guo, M. P. Haynes, T. M. Heckman, M. R. Krumholz, J. Lemonias, C. Li, S. Moran, N. Rodriguez-Fernandez, D. Schiminovich, K. Schuster, and A. Sievers, "COLD GASS, an IRAM legacy survey of molecular gas in massive galaxies - II. The non-universality of the molecular gas depletion time-scale," *Mon. Not. R. Astron. Soc.*, vol. 415, no. 1, pp. 61–76, 2011.

[26] K. M. Ferrière, "The interstellar environment of our galaxy," *Rev. Mod. Phys.*, vol. 73, no. 4, pp. 1031–1066, dec 2001.

[27] M.-M. Mac Low and R. S. Klessen, "Control of star formation by supersonic turbulence," *Rev. Mod. Phys.*, vol. 76, no. 1, pp. 125–194, jan 2004.

[28] R. C. Kennicutt, "STAR FORMATION IN GALAXIES ALONG THE HUBBLE SEQUENCE," *Annu. Rev. Astron. Astrophys.*, vol. 36, no. 1, pp. 189–231, sep 1998.

[29] G. team, "CLASS: Continuum and Line Analysis Single-dish Software," 2006. [Online]. Available: https://www.iram.fr/IRAMFR/GILDAS/doc/html/class-html/class.html

[30] C. Kramer, "Calibration of spectral line data at the IRAM 30m radio telescope," 1997. [Online]. Available: http://www.iram.es/IRAMES/mainWiki/Iram30mEfficiencies?action=AttachFile{&}do=get{&}target=cali{_}rep.pdf

[31] P. M. Solomon, D. Downes, S. J. E. Radford, and J. W. Barrett, "The Molecular Interstellar Medium in Ultraluminous Infrared Galaxies," *Astrophys. J.*, vol. 478, no. 1, pp. 144–161, mar 1997.

[32] P. Solomon and P. Vanden Bout, "Molecular Gas at High Redshift," *Annu. Rev. Astron. Astrophys.*, vol. 43, no. 1, pp. 677–725, sep 2005.

[33] G. E. Magdis, D. Rigopoulou, G. Helou, D. Farrah, P. Hurley, A. Alonso-Herrero, J. Bock, D. Burgarella, S. Chapman, V. Charmandaris, A. Cooray, Y. Sophia Dai, D. Dale, D. Elbaz, A. Feltre, E. Hatziminaoglou, J.-S. Huang, G. Morrison, S. Oliver, M. Page, D. Scott, and Y. Shi, "Mid- to far-infrared properties of star-forming galaxies and active galactic nuclei," *Astron. Astrophys.*, vol. 558, p. A136, oct 2013.